Environmental Science and Ecotechnology 31 (2026) 100686

Contents lists available at ScienceDirect

Environmental Science and Ecotechnology

journal homepage: www.journals.elsevier.com/environmental-science-and-ecotechnology/

Original Research

Microplastics accumulate in human bile and drive cholangiocyte senescence

Leilei Zhan [a,1], Li Fu [b,1], Qingli Zeng [c,1], Ruiyin Liang [d], Jinhui Tang [e], Juan Liu [a], Bo Qian [f,*], Zhe Xu [a,**], Lin Che [g,h,***]

[a] The Tenth Affiliated Hospital of Southern Medical University (Dongguan People's Hospital), Dongguan, 523059, China
[b] Tianhe District Center for Disease Control and Prevention, Guangzhou, 510655, China
[c] Department of Emergency Medicine, The First Affiliated Hospital, Sun Yat-sen University, Guangzhou, 510080, China
[d] The Philippine Women's University, Manila, 0900, Philippines
[e] Department of Pathophysiology, Guangdong Provincial Key Laboratory of Proteomics, and State Key Laboratory of Organ Failure Research, Southern Medical University, Guangzhou, 510515, China
[f] Guangxi Key Laboratory of Environmental Exposomics and Entire Lifecycle Health, School of Public Health, Guilin Medical University, Guilin, 541199, China
[g] State Key Laboratory of Oncology in South China, Sun Yat-sen University Cancer Center, Guangzhou, 510060, China
[h] Guangzhou National Laboratory, Guangzhou, 510005, China

ARTICLE INFO

Article history:
Received 24 May 2025
Received in revised form
24 March 2026
Accepted 26 March 2026

Keywords:
Microplastics
Multimodal detection
Mitochondrial dysfunction-associated senescence
Human bile
Health risks

ABSTRACT

Microplastics are ubiquitous environmental pollutants that increasingly infiltrate human organs and tissues through multiple exposure pathways. While acute toxicological impacts have been documented, the metabolic fate of these polymers within the enterohepatic circulation remains poorly understood. Bile serves as a critical excretory fluid, and disruptions in its balance can lead to biliary tract diseases such as gallstones. However, the long-term accumulation patterns and chronic toxic effects of microplastics within the human biliary system are largely unknown. Here we show the universal presence of microplastics in human bile. Using a multimodal analytical approach, we identified six polymer types, predominantly polyethylene terephthalate and polyethylene, occurring primarily as 20–50 μm particles. We demonstrate that chronic, low-dose exposure to these microplastics induces mitochondrial dysfunction-associated senescence in cholangiocytes. Notably, targeted antioxidant intervention with melatonin effectively preserves mitochondrial function and mitigates this microplastic-induced cytotoxicity. These findings reveal the biliary system as a major reservoir for microplastic accumulation and excretion. Furthermore, they provide a mechanistic foundation for assessing the health risks of plastic pollution and developing therapeutic interventions for environmentally driven biliary disorders.

1. Introduction

Plastics are widely used in modern manufacturing due to their cost-effectiveness and advantageous properties, including durability and corrosion resistance [1]. However, these same characteristics contribute to their environmental persistence. Global plastic production has led to widespread environmental contamination, with approximately 350 million metric tons of plastic waste generated in 2019. Projections suggest that this figure may exceed 1 billion metric tons annually by 2060 [2]. Mechanical abrasion, ultraviolet radiation, and biodegradation processes fragment plastic debris into microplastics (MPs), which have emerged as a novel class of environmental contaminants [3,4]. MPs are generally defined as plastic particles ranging from 1 μm to 5 mm in diameter. They are ubiquitous across atmospheric, terrestrial, and marine environments and have infiltrated the food chain [5–7]. Given their environmental persistence and potential health implications, MPs have become a critical subject of research

* Corresponding author.
** Corresponding author.
*** Corresponding author. State Key Laboratory of Oncology in South China, Sun Yat-sen University Cancer Center, Guangzhou, 510060, China.
E-mail addresses: soloqb@outlook.com (B. Qian), xu__zhe@163.com (Z. Xu), che_lin@gzlab.ac.cn (L. Che).
[1] These authors have contributed equally to this work.

https://doi.org/10.1016/j.ese.2026.100686

in environmental and health sciences [8,9].

A substantial body of prior research has primarily focused on the environmental distribution of MPs and their toxicological effects on aquatic organisms [10,11]. Human exposure has been increasingly investigated, with estimates suggesting that individuals may ingest between 39,000 and 52,000 MP particles annually through food consumption [12]. For example, European populations are estimated to ingest approximately 11,000 MP particles per year through bivalve consumption [13]. Additional assessments indicate that maximum daily intake via rice consumption may reach 1.292, 1.527, and 1.313 particles kg^{-1} d^{-1} for Indian males, females, and children, respectively. In Hong Kong, annual intake from packaged beverages has been estimated at approximately 6200 particles per adult, corresponding to an average consumption of 157.3 $\pm$ 209.7 L yr^{-1} [14,15]. Emerging evidence has identified MPs in various human tissues and biological samples, including the lungs, placenta, feces, brain, and semen, suggesting systemic exposure and distribution [16–20]. Experimental studies demonstrate that MPs can be internalized by human renal tubular epithelial cells, intestinal epithelial cells, and animal tissues, leading to oxidative stress, inflammatory responses, and histopathological alterations in organs such as the kidneys, intestines, and liver [21–24]. However, many toxicological studies employ exposure concentrations substantially exceeding environmentally relevant levels. Moreover, mechanistic studies predominantly rely on acute exposure models, which may not accurately reflect the chronic, low-dose exposures experienced by humans. These discrepancies limit the extrapolation of laboratory findings to real-world health risk assessment [12,25]. Accordingly, developing toxicological models that more closely simulate environmentally relevant exposure conditions is essential to improving the validity of risk evaluations.

Biliary tract diseases encompass a spectrum of disorders affecting the gallbladder and bile ducts, with gallstones representing the most prevalent condition. Gallstone formation is influenced by multiple factors, including genetic predisposition, dietary patterns, and obesity [26]. Bile functions not only as a lipid-rich digestive fluid but also as a critical excretory pathway in the enterohepatic circulation [27]. Disruptions in the balance of key biliary components—such as cholesterol, bilirubin, and bile acids—can lead to precipitation and crystallization within the gallbladder, ultimately resulting in gallstone formation [28,29]. Environmental contaminants, including heavy metals and organic solvents, may enter the human body via the food chain or airborne exposure, thereby influencing biliary health [30–32]. Notably, MPs, as emerging environmental pollutants, may directly affect digestive physiology following ingestion. Experimental evidence suggests that MPs can disrupt enterohepatic circulation, impair bile flow, and contribute to biliary dysfunction [33,34]. The physicochemical characteristics of bile, particularly its high concentrations of bile salts and lipids, may facilitate the adsorption of hydrophobic polymers, potentially influencing the distribution and retention of MPs in this milieu compared with hydrophilic biological fluids such as blood or amniotic fluid [35,36]. Therefore, detecting MPs in bile may provide novel insights into their metabolic fate and excretory pathways. This perspective implies that the biliary tract could be a major excretion route—a mechanism neglected by earlier studies focusing on accumulation in sites such as the placenta or lungs. Investigating the toxicological implications of MPs and their potential association with biliary diseases is of great importance for developing prevention and management strategies for gallstones and other biliary disorders.

Comprehensive characterization of MPs requires multimodal analytical approaches capable of determining particle size, morphology, and polymer composition [16]. Raman spectroscopy and Fourier-transform infrared microspectroscopy are commonly employed due to their chemical specificity and spatial resolution [37]. However, these technologies may be limited by signal interference, sample preparation constraints, and relatively low throughput. Pyrolysis–gas chromatography–mass spectrometry has emerged as a complementary thermal analytical technique capable of identifying and quantifying polymer types in complex matrices without size-based preselection [38]. Furthermore, laser direct infrared (LDIR) spectroscopy, characterized by its fully automated infrared chemical imaging capabilities, features a broad recognition range and significantly streamlines the assessment of MP size, shape, and polymer composition [39]. Additionally, scanning electron microscopy (SEM) provides high-resolution morphological analysis of MPs [40]. The multimodal detection approach addresses shortcomings across different technologies while providing an extensive characterization of MPs. Consequently, it enhances the precision of MP identification and quantification, thus establishing a more dependable foundation for environmental monitoring and risk assessment [41].

In this study, we employ a multimodal approach to assess and quantify the mass concentration, types, and physical characteristics of MPs in human bile. Furthermore, we explore the chronic cytotoxic effects of MPs, providing novel evidence for understanding MP-related health risks in the biliary system.

2. Methods

2.1. Human bile sample collection

We collected bile samples from patients undergoing laparoscopic cholecystectomy. Patients were included if they: (1) presented with typical upper abdominal pain and tenderness; (2) had imaging evidence of gallstones on magnetic resonance imaging (MRI) and/or computed tomography (CT); and (3) were aged 18 to 80 years. Exclusion criteria comprised: (1) non-calculous biliary diseases (e.g., strictures, tumors, parasitosis); (2) a history of prior biliary surgery (e.g., cholecystectomy, choledochojejunostomy); (3) severe comorbidities contraindicating surgery or endoscopy (e.g., liver or kidney failure, advanced malignancies); and (4) pregnancy or lactation. The cohort included five patients without gallstones and nine patients with gallstones. All participants were recruited from Dongguan People's Hospital and provided written informed consent prior to participation. The study protocol was approved by the Medical Ethics Committee of Dongguan People's Hospital (approval number KYKT2022-071) and was conducted in accordance with the principles of the Declaration of Helsinki.

To minimize potential plastic contamination, all experimental procedures strictly adhered to plastic-free protocols. Following established surgical procedures, bile samples (5 mL per patient) were collected in sterilized glass containers fitted with polytetrafluoroethylene-sealed lids. The samples were immediately transported to the laboratory on ice and stored at −80 °C until further analysis. Subsequent analytical procedures were performed by Shanghai Weipu Testing Technology Group Co., Ltd., China.

2.2. Sample preparation for MPs using pyrolysis–gas chromatography–mass spectrometry

Sample preparation of bile for MP analysis was performed using pyrolysis–gas chromatography–mass spectrometry (Py-GC/MS), following the method described by Marfella et al. [17]. Briefly, bile samples were placed in a 100-mL beaker to measure their wet weight (M_W). The samples were then dried in an oven at 60 °C until they reached a constant weight. Sequential solvent extraction was

conducted using three solvents. First, 10 mL of chloroform was added, and the mixture was sonicated for 10 min (repeated three times). The resulting extracts were transferred to a new beaker. Next, 10 mL of hexafluoroisopropanol was added, followed by sonication for 10 min (repeated three times), and the extracts were collected in a fresh beaker. Finally, 10 mL of xylene was added, and extraction was performed at 150 °C for 10 min (repeated three times). All extracts were subsequently combined in a new beaker (Supplementary Table S1). The combined extract was evaporated at 80 °C until a concentrate weight (M_C) of approximately 1.0 g was obtained. Using a glass Pasteur pipette, the concentrate was quantitatively transferred into a Py-GC/MS crucible. Following complete solvent evaporation, the sample loading weight (M_L) was determined before analysis using a Py-GC/MS system (GCMS-QP2020, Shimadzu Corporation, Japan). The total tested mass (M_{TT}, in grams) was calculated as follows: $M_{TT} = M_L/M_C \times M_W$.

2.3. MP analysis using Py-GC/MS

The concentrated bile samples were subjected to pyrolysis at 550 °C using a Frontier Lab EGA/PY-3030D system (Fukushima, Japan). The resulting pyrolysates were directly transferred to a GC-2030 gas chromatograph (Shimadzu Corp., Kyoto, Japan) equipped with an Rtx-5MS capillary column (30 m × 0.25 mm × 0.25 μm; Restek, USA). The GC temperature program was initiated at 40 °C (held for 2 min), ramped at 20 °C min^{-1} to 320 °C, and held for 14 min, resulting in a total run time of 30 min. Helium was used as the carrier gas at a linear velocity of 36.1 cm s^{-1}. Mass spectrometric detection was performed using a GCMS-QP2020 system (Shimadzu Corp., Kyoto, Japan) coupled to gas chromatography, operating with an ion source temperature of 230 °C and a mass scan range of *m/z* 29–600. Polymer identification was performed using LabSolutions software (version 4.45).

Standard reference materials were prepared for quantitative calibration. We analyzed eleven target polymers: polyamide 6 (PA6), polyamide 66 (PA66), polybutylene adipate terephthalate (PBAT), polycarbonate (PC), polyethylene (PE), polyethylene terephthalate (PET), polylactic acid (PLA), polymethyl methacrylate (PMMA), polypropylene (PP), polystyrene (PS), and polyvinyl chloride (PVC). Each polymer was identified based on its characteristic pyrolysis products, diagnostic ions, and specific retention times, with confirmation by comparison to the National Institute of Standards and Technology spectral library. Quantification of the identified MPs was performed using calibration curves generated from the corresponding polymer standards.

2.4. Processing of samples for MP analysis via LDIR spectroscopy and SEM

To further characterize the quantity, size distribution, and morphology of MP particles, we performed LDIR spectroscopy and SEM on bile samples. Sample preparation for LDIR analysis was modified from the method described by Wang et al. [42]. Briefly, bile samples were digested with 68% nitric acid at a bile-to-acid volume ratio of 1:3. The mixture was incubated at room temperature for 12 h, then heated on a graphite heating plate at 60 °C for 3 h to facilitate protein digestion. Following digestion, the solution was vacuum-filtered through a 13-μm stainless steel mesh (Shanghai Youmi Industrial Co., Ltd., China). The mesh retaining the suspected MPs was rinsed three times with ultrapure water and ethanol to remove residual digestion reagents. Next, the mesh was submerged in filtered anhydrous ethanol and subjected to ultrasonic treatment at 40 kHz for 30 min to detach the particles from the mesh and transfer them into the ethanol phase. The resulting suspension was concentrated to around 150 μL and dried in an infrared drying oven (Supplementary Table S2). The dried residue was transferred onto a low-emissivity microscope slide and allowed to air-dry completely. MP identification and characterization were performed using an Agilent 8700 LDIR spectrometer (Agilent Technologies Co., Ltd., China). Particles identified as MPs by LDIR were subsequently sputter-coated and examined using SEM to further assess their surface morphology.

2.5. Analysis of MPs using LDIR and SEM

We performed MP identification and particle characterization using the Agilent 8700 LDIR spectrometer (Agilent Technologies Co., Ltd., China). The instrument was operated in particle analysis mode to determine MP abundance and size distribution, following methods similar to those described in previous studies [43,44]. The analysis employed the MPs Starter 1.0_1_1_1_2 spectral library and an automated particle-detection protocol with established quality-control parameters (spectral match score >0.65; detectable particle size range: 20–500 μm). We subsequently examined particles identified as MPs by LDIR using an Apreo 2C SEM system (Thermo Fisher Scientific, USA) to assess their morphological characteristics.

2.6. Quality assurance and quality control

To ensure rigorous quality assurance and quality control, we adhered to a strict plastic-free principle throughout the entire experimental procedure. We prepared blank controls in accordance with the materials and instruments used. All reagents and solutions, including anhydrous ethanol, nitric acid, and analytical-grade Milli-Q® water, were vacuum-filtered three times through a 0.45-μm PTFE membrane prior to use to minimize potential contamination. For Py-GC/MS analysis, we implemented comprehensive quality control measures, including background contamination assessment through sampling, instrument, and reagent blanks (Supplementary Fig. S1–S5), spiking recovery experiments, and establishing detection and quantification limits. Similarly, strict procedural controls were applied during MP detection using LDIR spectroscopy (Supplementary Fig. S6). These results demonstrated that no MP signals were detected in any of the blank controls, indicating that contamination was effectively minimized throughout the experimental process.

2.7. Recovery experiment

We conducted a spiking recovery test to evaluate the analytical recovery of polymers from bile matrices. Given the widespread presence of MPs in the environment and their inevitable presence in biological samples, we added known concentrations of 11 MP solution types to bile samples. We calculated the recovery rate as $(m_s - m_o)/m_{sp} \times 100\%$, where m_s is the mass of MPs in the spiked sample, m_o is the mass of MPs in the original sample, and m_{sp} is the spiked amount. Recoveries ranged from 95.33% to 107.40%, indicating good performance of the method for the extraction, identification, and quantification of the 11 target MPs examined in this study (Supplementary Table S3). The results are consistent with previous studies employing similar methodologies [42,45].

2.8. Limits of detection and quantification

Limits of detection (LOD) and quantification (LOQ) for each target polymer were determined based on the procedural blank signal. Specifically, the LOD and LOQ were defined as 3 and 10 times the average signal of the procedural blanks, respectively (Supplementary Table S4). The LOD indicates the lowest detectable

concentration of a target polymer, whereas the LOQ signifies the minimum concentration that can be accurately quantified using the Py-GC/MS system.

2.9. Cell culture and treatments

Human biliary epithelial HuCCT1 cells were cultured in high-glucose Dulbecco's modified Eagle medium containing 10% fetal bovine serum (Gibco, USA) and 1% penicillin–streptomycin and maintained at 37 °C in a humidified atmosphere containing 5% CO_2. Spherical polystyrene nanoplastics (PS-NPs), polyethylene nanoplastics (PE-NPs), and polypropylene nanoplastics (PP-NPs), each with a nominal diameter of 100 nm, were purchased from Zhongke Keyou Technology (Beijing, China). To assess cytotoxicity, HuCCT1 cells were exposed to graded concentrations of PS-NPs, PE-NPs, and PP-NPs (0.02, 0.04, 0.08, 0.16, and 0.32 mg mL^{-1}) for three or seven days, and cell viability was evaluated using the 3-(4,5-dimethylthiazol-2-yl)-2,5-diphenyltetrazolium bromide (MTT) assay according to the manufacturer's instructions. Based on the dose–response results, a low concentration (0.04 mg mL^{-1}) was selected for subsequent experiments to simulate chronic exposure, and cells were continuously treated for seven days as the experimental endpoint.

2.10. Data-independent acquisition proteomics analysis

HuCCT1 cells and HuCCT1 cells treated with 0.1 mg mL^{-1} PS-NPs for seven days ($n = 3$ biological replicates per group) were subjected to data-independent acquisition (DIA) proteomics analysis. The analysis was performed by Shanghai Biotree Biotech (Shanghai, China). Differentially expressed proteins (DEPs) were identified using Student's *t*-test. Proteins with a fold change (FC) ≤ 0.83 or ≥ 1.2 and $P < 0.05$ were considered significantly differentially expressed. Bioinformatics analysis of the proteomics data mainly included principal component analysis (PCA), Gene Ontology (GO) functional enrichment analysis, and Kyoto Encyclopedia of Genes and Genomes (KEGG) pathway enrichment analysis. Protein–protein interaction (PPI) network analysis was performed by the STRING database (Search Tool for the Retrieval of Interacting Genes, https://cn.string-db.org/).

2.11. PS-NPs exposure and senescence-associated genes

We retrieved senescence-associated genes from the CellAge database (https://www.genomics.senescence.info/), a curated repository of human aging-related genes validated through genetic manipulation experiments and gene expression profiling. We performed Venn diagram analysis to identify overlapping genes between PS-NP-induced differentially expressed molecules and the senescence-associated gene set, thereby identifying a set of commonly associated genes.

2.12. Western blot

Protein samples extracted from cells were separated by sodium dodecyl sulfate–polyacrylamide gel electrophoresis and subsequently transferred onto polyvinylidene fluoride membranes. The membranes were then incubated overnight at 4 °C with primary antibodies, followed by 1 h of incubation at room temperature with secondary antibodies. Protein bands were visualized using an Azure C400 imaging system, and band intensities were measured using ImageJ software.

2.13. SA-β-gal staining

After treating HuCCT1 cells with PS-NPs alone or in combination with melatonin (MT) for seven days, we removed the culture medium. Briefly, the cells were treated with 1 mL of cell fixation solution at room temperature for 15 min, followed by overnight incubation in β-gal staining solution at 37 °C. Then, the cells were washed three times with PBS and imaged under an optical microscope. ImageJ software was used to quantify the number of β-gal-positive cells.

2.14. Flow cytometry

After cell treatment, the samples were fixed in 75% ice-cold ethanol, treated with RNase A, and stained with propidium iodide (PI). DNA content was analyzed using a Beckman Coulter flow cytometer, and the cell cycle distribution was quantified.

2.15. Immunofluorescence staining

HuCCT1 cells were treated with PS-NPs or melatonin for seven days. The cells were then fixed with 4% PFA and permeabilized with 0.5% Triton X-100 for 5 min. After permeabilization, cells were blocked with 1% BSA for 1 h at room temperature. Subsequently, the sections were incubated with primary antibodies overnight at 4 °C, followed by incubation with fluorescent secondary antibodies for 1 h at room temperature. 4′,6-diamidino-2-phenylindole was utilized for nucleus staining for 3 min. Fluorescence imaging was performed using a laser-scanning confocal microscope (Leica SP8, Germany).

2.16. Statistical analysis

We employed descriptive statistics to assess the demographic features of the participants. Continuous variables exhibiting normal and skewed distributions were summarized using means (standard deviation, SD) and medians (interquartile range, IQR), respectively. Categorical variables were represented by numbers and percentages. The normality of distribution for continuous variables was formally assessed using the Shapiro–Wilk test. To evaluate differences in MP concentrations across groups, the appropriate statistical test was selected based on this assessment: the unpaired *t*-test was used for normally distributed data, while the Mann–Whitney *U* test was used for non-normally distributed data. Experimental data are presented as mean ± SD. Intergroup comparisons were performed using Student's *t*-test for two groups and one-way analysis of variance (ANOVA) for multiple groups. All statistical calculations were executed using Statistical Package for the Social Sciences (SPSS) version 25.0 or GraphPad Prism 8.0. Differences were considered statistically significant at $P < 0.05$.

3. Results

3.1. Demographic characteristics

The clinical characteristics of the patients are detailed in Table 1. A total of 14 individuals were included in this study, comprising five participants in the non-gallstone control group (CG) and nine participants in the gallstone group (GG), as confirmed by MRI and/or CT examinations (Supplementary Fig. S7). The average age of the participants was 56.29 years, with a balanced distribution of males and females. Three patients (21.43%) reported a history of alcohol consumption, while one patient (7.14%) had a history of smoking. Four patients (28.57%) were from rural areas, whereas ten patients (71.43%) resided in

Table 1
Demographic characteristics of the participants in this study.

Characteristics	Total [*n* (%)]	CG [*n* (%)]	GG [*n* (%)]	*t*	*P*
Total	14 (100)	5 (35.71)	9 (64.29)		
Age (years) [Mean (SD)]	56.29 (14.45)	57.80 (17.60)	55.44 (13.49)	0.282	0.783[a]
Sex					1.000[b]
Male	7 (50.00)	3 (60.00)	4 (44.44)		
Female	7 (50.00)	2 (40.00)	5 (55.56)		
Drinking					1.000[b]
Yes	3 (21.43)	1 (20.00)	2 (22.22)		
No	11 (78.57)	4 (80.00)	7 (77.78)		
Smoking					1.000[b]
Yes	1 (7.14)	0 (0)	1 (11.11)		
No	13 (92.86)	5 (100.00)	8 (88.89)		
Residential area					0.221[b]
Rural	4 (28.57)	0 (0)	4 (44.44)		
Urban	10 (71.43)	5 (100.00)	5 (55.56)		
Frequency of using bottled water					0.086[b]
≥5 times week^{-1}	5 (35.71)	0 (0)	5 (55.56)		
<5 times week^{-1}	9 (64.29)	5 (100.00)	4 (44.44)		
Frequency of eating takeaway foods					0.580[b]
Never	9 (64.29)	4 (80.00)	5 (55.56)		
≤3 times week^{-1}	5 (35.72)	1 (20.00)	4 (44.44)		
BMI (kg m^{-2})					0.790[b]
Normal weight (≤23.9)	5 (35.71)	1 (20.00)	4 (44.44)		
Overweight (24.0–27.9)	7 (50.00)	3 (60.00)	4 (44.44)		
Obesity (≥28.0)	2 (14.29)	1 (20.00)	1 (11.12)		
Hypertension					0.221[b]
Yes	4 (28.57)	0 (0)	4 (44.44)		
No	10 (71.43)	5 (100.00)	5 (55.56)		
Diabetes					0.505[b]
Yes	2 (14.29)	0 (0)	2 (22.22)		
No	12 (85.71)	5 (100.00)	7 (77.78)		
Hyperlipidemia					0.580[b]
Yes	5 (35.71)	1 (20.00)	4 (44.44)		
No	9 (64.29)	4 (80.00)	5 (55.56)		
Hyperuricemia					1.000[b]
Yes	2 (14.29)	1 (20.00)	1 (11.12)		
No	12 (85.71)	4 (80.00)	8 (88.88)		
Cardiovascular disease					0.580[b]
Yes	4 (28.57)	2 (60.00)	2 (22.22)		
No	10 (71.43)	3 (40.00)	7 (77.78)		

Note: CG, non-gallstones group (control group); GG, gallstones group.
[a] Independent-sample *t*-test.
[b] Fisher's exact test.

urban areas. Five patients (35.71%) reported using plastic water bottles more than six times per week, whereas nine patients (64.29%) reported lower use. Nine patients (64.29%) reported never consuming takeout food, while five patients (35.71%) consumed takeout 1–3 times per week. In terms of weight classification, five patients (35.71%) were normal weight, seven (50%) were overweight, and two (14.29%) were obese. In addition, four patients (28.57%) had hypertension, two (14.29%) had type 2 diabetes, five (35.72%) had hyperlipidemia, two (14.29%) had hyperuricemia, and four (28.57%) had cardiovascular disease.

3.2. Clinical characteristics

The clinical indicators are detailed in Supplementary Table S5. In the GG group, the average values for alanine transaminase (ALT), total bilirubin (TBIL), direct bilirubin (DBIL), and indirect bilirubin (IBIL) were recorded as 354.2 ± 261.08 U L^{-1}, 84.60 ± 58.68 μmol L^{-1}, 47.54 ± 34.73 μmol L^{-1}, and 37.11 ± 24.49 μmol L^{-1}, respectively. Aspartate transaminase (AST) levels were markedly elevated in the patient group, with a median of 180.00 U L^{-1} (IQR, 66.00–246.00), and liver function indices were significantly higher than those in the CG group, including ALT (19.80 ± 5.59 U L^{-1}; independent-sample *t*-test, $P = 0.005$), AST (23.60 ± 4.16 U L^{-1}; Mann–Whitney *U* test, $P = 0.014$), TBIL (18.32 ± 5.90; independent-sample *t*-test, $P = 0.009$), DBIL (12.52 ± 0.99; independent-sample *t*-test, $P = 0.005$), and IBIL (12.52 ± 2.97; independent-sample *t*-test, $P = 0.017$). However, no significant difference in bile acids was observed between the two groups (8.40 ± 21.67 vs. 79.00 (9.00, 257.00), Mann–Whitney *U* test, $P = 0.081$).

3.3. Detection rate of MPs in human bile

A total of 14 human bile samples were collected, including five control bile samples from individuals without gallstones (CB group) and nine samples from patients with gallstones (GB group). To assess the types and concentrations of MPs in human bile, Py-GC/MS was used to identify MPs across eleven representative polymer types. Based on the types of MPs detected, the analysis was conducted using the spectra of standard samples as positive controls (Supplementary Table S6 and Fig. S8). Py-GC/MS analysis revealed the presence of MPs in all bile samples (Fig. 1a). Among the 11 polymer categories examined, six types of MPs were identified, with a predominance of PET (68.05%) and PE (27.11%). Other identified polymers included PS (0.87%), PP (1.44%), PVC (1.17%), and PA66 (1.35%) (Fig. 1b).

The total concentration of MPs was slightly higher in individuals under 60 years of age compared to those 60 years and

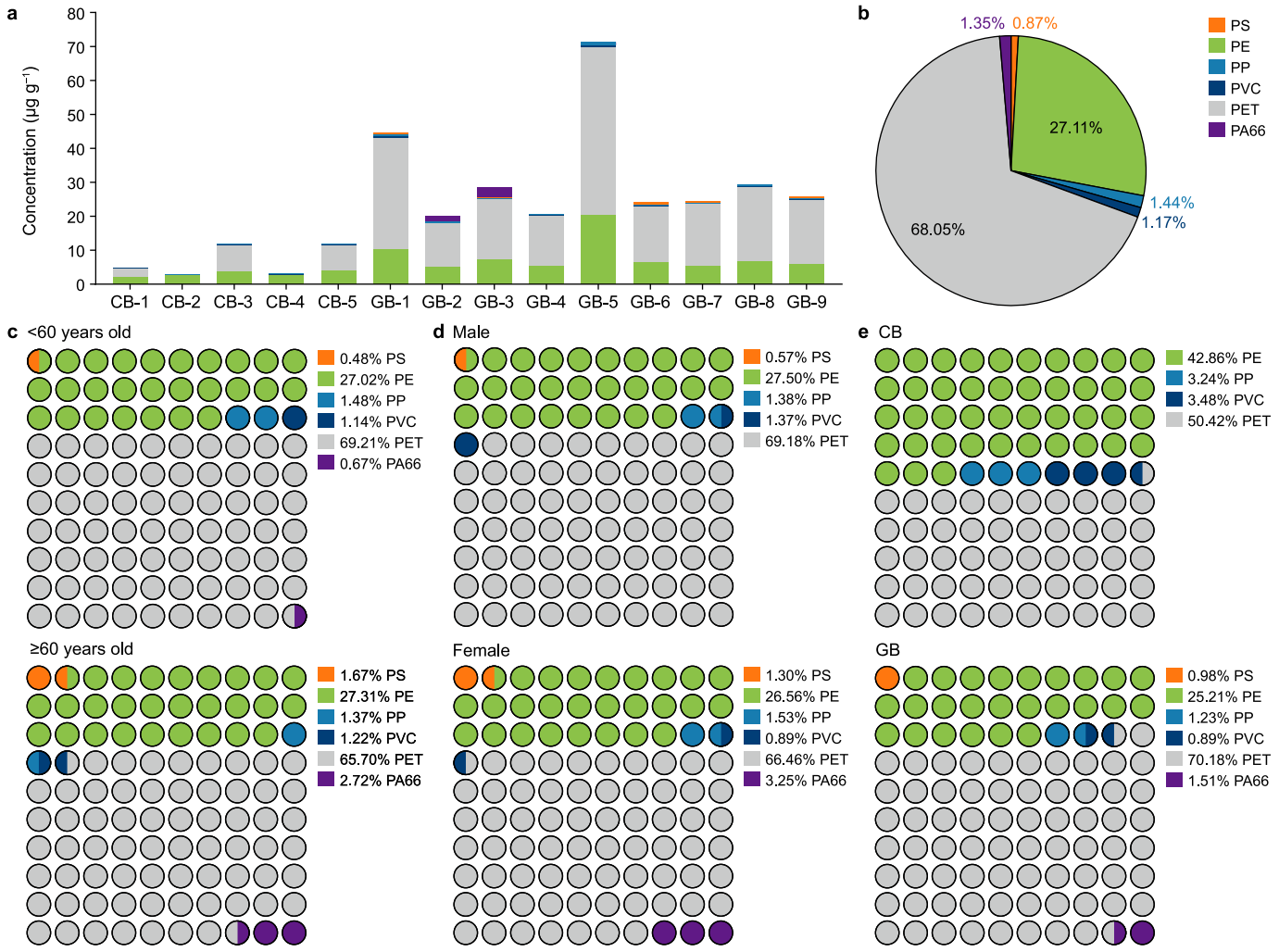

Fig. 1. Characteristics of human bile microplastics (MPs) detected by pyrolysis–gas chromatography–mass spectr**ometry. a,** Concentration of MPs classified by type of polymer in each human bile sample. **b,** Distribution of MP particles in all human bile samples. **c,** Distribution of MP particles in individuals aged <60 and ≥ 60 years **d,** Distribution of MP particles in males and females. **e,** Distribution of MP particles in the CB and GB groups. CB, control bile from individuals without gallstones; GB, bile from patients with gallstones; PA66, polyamide 66; PET, polyethylene terephthalate; PVC, polyvinyl chloride; PP, polypropylene; PE, polyethylene; PS, polystyrene.

older (Fig. 1c). In the <60 age group, the proportional contributions of PS, PE, PP, PVC, PET, and PA66 were 0.48%, 27.02%, 1.48%, 1.14%, 69.21%, and 0.67%, respectively. In contrast, among individuals aged 60 and above, the proportions of PS, PE, PP, PVC, PET, and PA66 were 1.67%, 27.31%, 1.37%, 1.22%, 65.71%, and 2.72%, respectively (Fig. 1c). Furthermore, the concentration of MPs was marginally higher in males than in females (Fig. 1d). In males, PS, PE, PP, PVC, and PET accounted for 0.57%, 27.50%, 1.38%, 1.37%, and 69.18% of the total concentration, respectively. In females, the proportions of PS, PE, PP, PVC, PET, and PA66 were 1.30%, 26.56%, 1.53%, 0.89%, 66.46%, and 3.25%, respectively (Fig. 1d).

The distribution of polymers in the samples was not uniform (Table 2). All samples contained PE and PP, while PS and PA66 were found exclusively in the GB group samples. Notably, PS was present in 66.7% of the GB group. PVC was detected in 100% of the CB group and 77.8% of the GB group. Meanwhile, PET was observed in 60.0% of the CB group and in all samples of the GB group. PA66 was detected in only 22.2% of the GB group. The total concentration of MPs in the GB group was significantly greater than that in the CB group (Fig. 1e). In the GB group, PE, PP, PVC, and PET accounted for 42.86%, 3.24%, 3.48%, and 50.42% of the total concentration, respectively. In contrast, in the CB group, the proportional contributions of PS, PE, PP, PVC, PET, and PA66 were 0.98%, 25.21%, 1.23%, 0.89%, 70.18%, and 1.51%, respectively (Fig. 1e).

3.4. Differences in MP concentrations between the CB and GB groups

The results of the study indicate that there were no significant differences in MP concentrations when groups were classified by age or gender (Fig. 2a and b; Supplementary Fig. S9). In the CB group, the total concentration of MPs detected in bile ranged from 3.00 to 11.95 μg g^{-1}, with a median concentration of 4.82 μg g^{-1}. In contrast, the GB group exhibited a total MP concentration in bile ranging from 20.02 to 71.22 μg g^{-1}, with a median concentration of 25.89 μg g^{-1}. The concentrations of PS, PE, PP, PVC, PET, and PA66 are detailed in Table 3. The results revealed that the MP concentration in the GB group was significantly higher than that in the CB group (25.89 [24.26–29.30] vs. 6.98 ± 4.56, Mann–Whitney *U* test, $P < 0.001$) (Table 4 and Fig. 2c–i). Furthermore, PS and PA66 were exclusively detected in the GB group, with concentrations of 0.47 ± 0.27 and 2.19 ± 1.04, respectively. The concentrations of PE and PET in the GB group were also higher than those in the CB group (6.49 [5.34, 7.22] vs. 2.99 ± 0.80, Mann–Whitney *U* test,

Table 2
Rates of MPs detection in CB and GB.

Variables	Detection rates of MPs		
	Overall ($n = 14$)	CB ($n = 5$)	GB ($n = 9$)
PS	42.9% (6/14)	0 (0/5)	66.7% (6/9)
PE	100.0% (14/14)	100.0% (5/5)	100.0% (9/9)
PP	100.0% (14/14)	100.0% (5/5)	100.0% (9/9)
PVC	85.7% (12/14)	100.0% (5/5)	77.8% (7/9)
PET	85.7% (12/14)	60.0% (3/5)	100.0% (9/9)
PA66	14.3% (2/14)	0 (0/5)	22.2% (2/9)

Note: CB, control bile from individuals without gallstones; GB, bile from patients with gallstones; PS, polystyrene; PE, polyethylene; PP, polypropylene; PVC, polyvinyl chloride; PET, polyethylene terephthalate, PA66, polyamide 66. Values in parentheses represent the number of positive samples/total number of samples in the corresponding group.

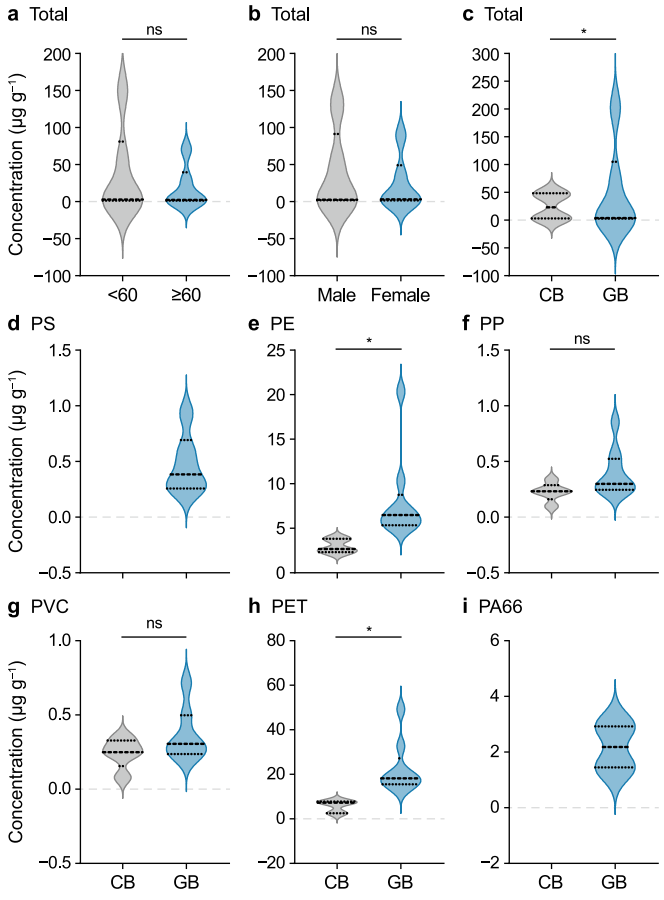

Fig. 2. Differences in microplastic (MP) concentrations between different **groups. a,** Concentrations of total MPs in individuals aged <60 and ≥ 60 years **b,** Concentrations of total MPs in the male and female. **c,** Concentrations of total MPs in the CB and GB. **d–i,** Concentrations of PS (**d**), PE (**e**), PP (**f**), PVC (**g**), PET (**h**), and PA66 (**i**) in the CB and GB. The three horizontal dashed lines, from bottom to top, represent the positions of the 25th percentile (Q1, lower quartile), the median (Median), and the 75th percentile (Q3, upper quartile), respectively. *$P < 0.01$. "ns" indicates no statistical significance between groups. CB, control bile from individuals without gallstones; GB, bile from patients with gallstones; PS, polystyrene; PE, polyethylene; PP, polypropylene; PVC, polyvinyl chloride; PET, polyethylene terephthalate; PA66, polyamide 66.

$P < 0.001$; 18.21 [16.23, 21.69] vs. 5.86 ± 2.90, Mann–Whitney U test, $P = 0.009$). However, no significant differences in PP and PVC concentrations were observed between the two groups. In summary, these findings indicate that bile from patients with gallstones contains significantly higher levels of MPs compared with controls. Nevertheless, this association requires further validation in studies with larger sample sizes.

3.5. Physical characteristics of MPs

To characterize the physical properties of bile MPs, we employed LDIR spectroscopy. This technique identified 32 distinct polymer types among the MPs, with PA the most prevalent, accounting for 29.57% of the total. The next most common polymers included acrylic polymers (ACR, 15.74%), chlorinated paraffins (CPE, 15.44%), polyurethanes (PU, 8.07%), butadiene rubber (BR, 4.54%), PET (3.63%), PVC (3.33%), fluorocarbon rubber (FKM, 2.52%), PE (2.02%), PLA (1.72%), PMMA (1.72%), PP (1.21%), styrene-butadiene rubber (SBR, 1.21%), acrylonitrile-butadiene-styrene copolymer (ABS, 1.11%), and polysulfone (PSF, 1.01%). The remaining 17 polymer types collectively accounted for 7.15% of the total MPs (Fig. 3a; Supplementary Fig. S10). The detected MP sizes in bile ranged from 20.34 to 451.97 μm. Specifically, the majority (86.42%) of the MPs were found to be between 20 and 50 μm, while 9.15% measured between 50 and 100 μm, and 4.43% exceeded 100 μm (Fig. 3b). The three most abundant polymers, PA, ACR, and CPE, had average particle diameters (based on width and length measurements) of 46.14, 26.72, and 36.43 μm, respectively (Fig. 3c). Additional parameters such as perimeter, width, height, area, and aspect ratio (width/height) (Fig. 3d–h). Further calculations included eccentricity (focus-to-distance/line-to-distance), circularity ($4\pi A/P^2$, where A is the area and P is the perimeter), and volume (area/convex area), revealing notable variations in the shape and density of the identified MPs (Fig. 3i–k). To explore the morphological features, SEM imaging was subsequently applied to six polymer types identified in bile samples previously analyzed with LDIR spectroscopy (Fig. 4). Under SEM, irregular, rod-shaped, and spherical MPs were observed (Fig. 4a–f).

3.6. Characteristics of PS-NPs and their effects on cell viability

To investigate the toxic effects of MPs on cholangiocytes, PS-NPs were chosen as representative test materials, and their properties were first characterized. PS-NPs were dispersed in a cell culture medium and analyzed using transmission electron microscopy. PS-NPs exhibited a spherical morphology with a uniform size distribution (Fig. 5a). Dynamic light scattering measurements indicated an average hydrodynamic diameter of 102.5 nm (Fig. 5b). Subsequently, the low-concentration exposure (0.04 mg mL^{-1}) reflected typical aquatic environmental levels of NPs from anthropogenic sources and secondary production [46]. Cell viability assays demonstrated time- and concentration-dependent decreases in the viability of HuCCT1 cells exposed to PS-NPs for three and seven days (Fig. 5c and d). To simulate chronic low-dose human exposure, HuCCT1 cells were treated with 0.04 mg mL^{-1} PS-NPs for seven days, and this condition was selected for subsequent experiments.

3.7. Proteomic analysis of chronic low-dose PS-NPs exposure–induced cellular senescence

To investigate the effects of PS-NP exposure on protein expression and toxicity in cholangiocytes, we performed data-independent acquisition proteomic analysis. The experimental workflow encompassed cell sample preparation, Liquid chromatography-tandem mass spectrometry analysis, and bioinformatics processing (Fig. 6a). Correlation analysis between samples revealed a strong association ($r = 0.99$) (Fig. 6b). Compared with the control (Ctrl) group, PS-NPs exposure resulted in the downregulation of 425 proteins and upregulation of 197 proteins

Table 3
Concentrations of MPs in CB and GB.

Variables	Concentration (μg g^{-1})													
	CB							GB						
	Total MPs	PS	PE	PP	PVC	PET	PA66	Total MPs	PS	PE	PP	PVC	PET	PA66
Minimum	3.00	-	2.11	0.10	0.08	2.53	-	20.02	0.25	5.09	0.22	0.21	12.95	1.45
Maximum	11.95	-	4.02	0.34	0.35	7.80	-	71.22	0.93	20.36	0.85	0.72	49.29	2.92
Mean	6.98	-	2.99	0.23	0.24	5.86	-	32.08	0.47	8.09	0.39	0.37	22.51	2.19
SD	4.56	-	0.80	0.08	0.10	2.90	-	16.37	0.27	4,87	0.21	0.18	11.53	1.04
25% percentile	3.25	-	2.52	0.22	0.23	4.89	-	24.26	0.27	5.34	0.27	0.25	16.23	1.82
50% percentile	4.82	-	2.67	0.23	0.25	7.25	-	25.89	0.38	6.49	0.30	0.31	18.21	2.19
75% percentile	11.86	-	3.63	0.24	0.30	7.53	-	29.30	0.57	7.22	0.47	0.41	21.69	2.55
IQR	8.61	-	1.10	0.02	0.07	2.64	-	5.04	0.30	1.88	0.20	0.16	5.45	0.74

Note: CB, control bile from individuals without gallstones; GB, bile from patients with gallstones; PS, polystyrene; PE, polyethylene; PP, polypropylene; PVC, polyvinyl chloride; PET, polyethylene terephthalate; PA66, polyamide 66. SD, standard deviation; IQR, interquartile range.

Table 4
Comparative analysis of MPs concentration in CB and GB.

MPs	Combined (CB + GB)	CB	GB	t/U	*P*
Total MPs	22.44 (11.89, 27.87)	6.98 ± 4.56	25.89 (24.26, 29.30)	45.00[a]	<0.001[a]
PS	0.47 ± 0.27	-	0.47 ± 0.27	-	-
PE	5.33 (3.73, 6.73)	2.99 ± 0.80	6.49 (5.34, 7.22)	45.00[a]	<0.001[a]
PP	0.27 (0.23, 0.35)	0.23 ± 0.08	0.30 (0.27, 0.47)	35.00[a]	0.112[a]
PVC	0.32 ± 0.16	0.24 ± 0.10	0.37 ± 0.18	1.50[b]	0.165[b]
PET	18.35 ± 12.45	5.86 ± 2.90	18.21 (16.23,21.69)	27.00[a]	0.009[a]
PA66	2.19 ± 1.04	-	2.19 ± 1.04	-	-

Note: CB, control bile from individuals without gallstones; GB, bile from patients with gallstones; PS, polystyrene; PE, polyethylene; PP, polypropylene; PVC, polyvinyl chloride; PET, polyethylene terephthalate; PA66, polyamide 66. Data are presented as median (interquartile range, IQR) or mean ± standard deviation, depending on the distributional characteristics of each variable.
[a] Mann–Whitney *U* Test.
[b] Independent-sample *t*-test.

(Fig. 6c; Supplementary Fig. S11). KEGG pathway enrichment analysis revealed significant alterations in pathways related to metabolism, the cell cycle, and cancer-related signaling (Fig. 6d). Notably, the intersection of PS-NPs-induced differentially expressed proteins with the CellAge database identified 25 senescence-associated molecules via Venn analysis (Fig. 6e). PPI network analysis further revealed that PS-NPs-regulated proteins were involved in lipid metabolism, transcriptional regulation, and cell cycle processes, including upregulated genes (e.g., *BHLHE40*, *CDKN1B, G6PD*) and downregulated genes (e.g., *AURKA*) (Fig. 6f and g). Collectively, our omics data demonstrate that chronic low-dose PS-NP exposure may induce cellular senescence.

3.8. Chronic low-dose PS-NPs exposure–induced cellular senescence

Fluorescence analysis showed that the cellular uptake of 0.04 mg mL^{-1} PS-NPs was significantly enhanced after 2 h (Fig. 7a). To investigate the effects of PS-NPs exposure on senescence in HuCCT1 cells, we treated the cells with 0.04 mg mL^{-1} PS-NPs for seven days. Western blot analysis, consistent with our previous proteomics data, demonstrated that PS-NP exposure significantly upregulated the expression of senescence-associated proteins BHLHE40 and CDKN1B (Fig. 7b and c). Assessment using SA-β-gal staining, a well-established senescence marker, revealed a significant increase in SA-β-gal (Fig. 7d and e). To evaluate the universality of PS-NPs-induced cellular senescence across different polymer types, we established an exposure model using MPs, specifically PE and PP. Chronic low-dose exposure to either PE or PP induced no significant cytotoxicity but resulted in an observable senescent phenotype (Supplementary Fig. S12). These findings suggest that MPs of various polymer types may contribute to cellular senescence. Flow cytometric analysis further confirmed that PS-NP exposure induced a prominent G1-phase cell cycle arrest, whereas apoptosis levels showed no significant change (Fig. 7e,f,h,i). These findings demonstrate that chronic low-dose PS-NP exposure induces senescence by upregulating senescence-associated proteins, enhancing SA-β-gal activity, and triggering cell cycle arrest (Fig. 7j).

3.9. Melatonin reverses chronic low-dose PS-NPs exposure–induced cellular senescence by inhibiting mitochondrial damage

To elucidate the molecular mechanisms underlying chronic low-dose PS-NPs exposure–induced cholangiocyte senescence, we first conducted a systematic GO analysis of differentially expressed proteins. The results demonstrated significant enrichment of these proteins in multiple mitochondria-related pathways, including regulation of mitochondrial adenosine triphosphate (ATP) synthesis coupled with electron transport, negative regulation of mitochondrial fusion, and negative regulation of mitochondrial cytochrome *c* release (Fig. 8a). Melatonin functions as a mitochondrial-targeted antioxidant, effectively scavenging mitochondrial reactive oxygen species (ROS) and exerting anti-inflammatory effects [47,48]. Previous studies have documented its protective effects against mitochondrial dysfunction in aging and neurodegenerative diseases [49,50]. However, its potential protective role against PS-NPs-induced cholangiocyte toxicity remains unclear. HuCCT1 cells were treated with PS-NPs, with or without melatonin (20 μM) co-treatment, for seven days. Results revealed that PS-NPs exposure significantly reduced cellular ATP levels (Fig. 8b), increased mitochondrial ROS production (Fig. 8c), promoted mitochondrial translocation of the fission protein Drp1

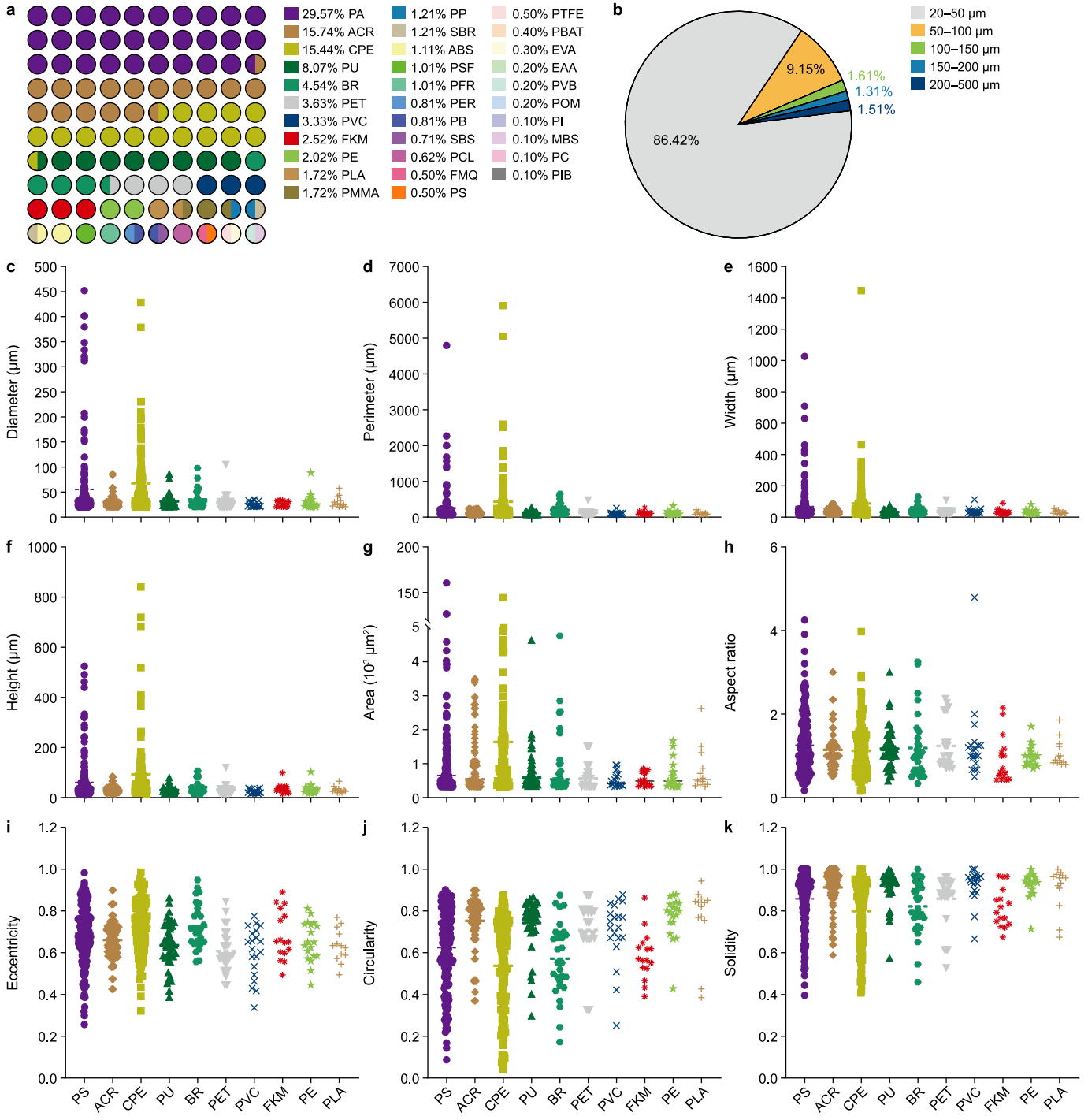

Fig. 3. Laser direct infrared (LDIR) imaging analysis of the physical properties of microplastics (MPs) in human **bile. a,** Type and abundance of MPs detected by LDIR. **b,** Size distribution of the detected MPs. **c–k,** Diameter (**c**), perimeter (**d**), width (**e**), height (**f**), area (**g**), aspect ratio (**h**), eccentricity (**i**), circularity (**j**), and solidity (**k**) of the top ten polymer types ranked by abundance: PA, ACR, CPE, PU, BR, PET, PVC, FKM, PE, and PLA. PA, polyamide; ACR, acrylate polymer; CPE, chlorinated polyethylene; PU, polyurethane; BR, butadiene rubber; PET, polyethylene terephthalate; PVC, polyvinylchloride; FKM, fluororubber; PE, polyethylene; PLA, polylactic acid; PMMA, polymethyl methacrylate; PP, polypropylene; SBR, polymerized styrene butadiene rubber; ABS, acrylonitrile butadiene styrene; PSF, polysulfones; PFR, phenol-formaldehyde resin; PER, Phenolic epoxy resin; PB, polybutadiene; SBS, styrene-butadiene-styrene; PCL, polycaprolactone; FMQ, fluorosilicone rubber; PS, polystyrene; PTFE, polytetrafluoroethylene; EVA, ethylene vinyl acetate copolymer; EAA, ethylene acrylic acid; PVB, polyvinyl butyral; POM, polyoxymethylene; PI, polyimide; MBS, methyl methacrylate-butadiene-styrene; PC, polycarbonate; PIB, polypropylene.

(Fig. 8d), and decreased mitochondrial membrane potential (Fig. 8e) in cholangiocytes compared to the Ctrl group. Notably, melatonin treatment effectively ameliorated these PS-NPs-induced mitochondrial dysfunction (Fig. 8b–e).

Furthermore, SA-β-gal staining analysis showed that melatonin significantly reduced the proportion of SA-β-gal-positive cells in PS-NPs-exposed groups (Fig. 9a and b). Evaluation of the senescence-associated secretory phenotype (SASP) demonstrated

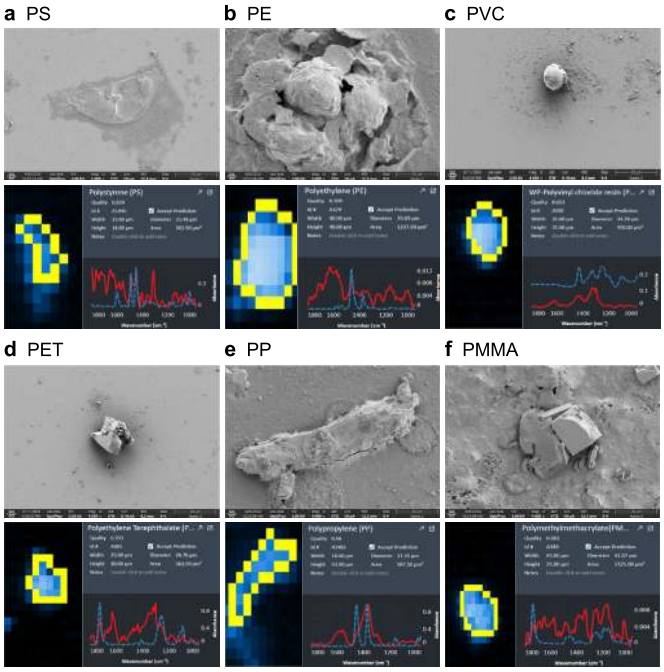

Fig. 4. Microphotographs of microplastics (MPs) found in human bile using laser direct infrared and scanning electron m**icroscopy.** Representative images of PS (**a**), PE (**b**), PVC (**c**), PET (**d**), PP (**e**), and PMMA (**f**). Scale bar: 20 μm. PS, polystyrene; PE, polyethylene; PVC, polyvinylchloride; PET, polyethylene terephthalate; PP, polypropylene; PMMA, polymethylmethacrylate.

that chronic low-dose PS-NPs exposure markedly upregulated both transcriptional and protein expression levels of IL-6 and TNF-α, while melatonin treatment significantly suppressed the expression of these senescence-related factors (Fig. 9c–e). Collectively, these findings demonstrate that chronic low-dose PS-NP exposure induces cholangiocyte senescence through mitochondrial dysfunction, whereas melatonin exerts pronounced cytoprotective effects by preserving mitochondrial function (Fig. 9f).

4. Discussion

In the present study, we employed a multimodal analytical approach to detect MPs in human bile for the first time. We systematically characterized the mass concentration, polymer types, and physicochemical properties of MPs in bile samples. Notably, significantly higher levels of MPs were observed in the gallstone group compared with the control group (25.89 [24.26–29.30] μg g^{-1} vs. 6.98 ± 4.56 μg g^{-1}, $P < 0.001$). Further investigations revealed that chronic low-dose MP exposure induces mitochondrial dysfunction–associated senescence (MiDAS). Importantly, melatonin effectively mitigated this toxic effect, suggesting a potential intervention strategy against MP-induced health hazards.

As increasing evidence indicates that MPs accumulate in various human organs and tissues, concerns regarding their potential health risks have intensified, underscoring the need for a more comprehensive understanding of their biological impacts [9,51,52]. The complexity of biological samples, diversity of polymer types, and high analytical costs have prompted the scientific community to develop a range of analytical approaches to facilitate the comprehensive identification and characterization of MPs under diverse conditions. Unlike spectroscopy-based techniques such as FTIR and Raman spectroscopy, Py-GC/MS can detect and quantify a wide range of MPs without a practical lower limit on particle size [53,54].

In this study, we integrated Py-GC/MS, LDIR, and SEM to systematically characterize MPs in human bile. However, each technique presents inherent limitations and differences in detection thresholds. Py-GC/MS provides highly sensitive absolute quantification across a wide range of polymers, with detection limits of 0.02–0.05 μg and recovery rates exceeding 95%. However, it does not offer information on particle number, morphology, or size distribution, thereby limiting particle-level characterization. LDIR microscopy enables high-throughput morphological analysis and polymer identification, yet its detection capability is constrained by particle size; under optimal conditions, it reliably detects particles ≥5 μm. Its sensitivity may also be reduced for dark-colored particles, hydrated samples, and polymers not present in the spectral library, potentially leading to underestimation of smaller MPs or to false-positive identification. SEM provides nanoscale morphological details (with a detection limit of approximately 0.1 μm) but cannot independently confirm polymer chemistry. Its narrow field of view and low analytical efficiency also necessitate preliminary chemical identification by techniques such as LDIR to avoid misclassifying natural fibers as MPs. Therefore, by adopting a synergistic multimodal approach—using LDIR for rapid screening and localization, SEM for detailed morphological characterization, and Py-GC/MS for precise chemical quantification—we effectively compensated for the limitations of each individual technique. This integrative approach enabled a comprehensive and accurate characterization of the complex properties of MPs in human bile.

The primary routes of human exposure to MPs include inhalation, ingestion, and dermal contact. Small MPs (e.g., PE and PP) have been detected in lung tissue from human autopsies, suggesting potential respiratory risks [55]. In children, fecal MPs (PVC, PET, and PE) have been associated with reduced gut microbiota diversity, particularly affecting *Parabacteroides* and *Alistipes* [45]. Patients with liver cirrhosis exhibit higher MP accumulation (PS,

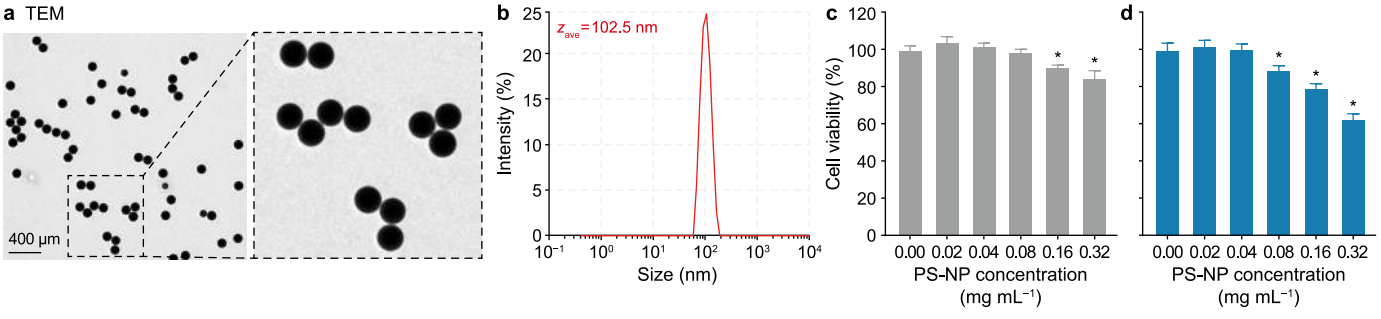

Fig. 5. Characteristics of polystyrene nanoplastics (PS-NPs) and their effects on cell via**bility. a,** Transmission electron microscopy images (TEM) of PS-NPs. Scale bar: 400 μm **b,** The size distribution of PS-NPs. **c**,**d**, The viability of HuCCT1 cells treated with PS-NPs was assessed by 3-(4,5-dimethylthiazol-2-yl)-2,5-diphenyltetrazolium bromide (MTT) assay. HuCCT1 cells were treated with different doses of PS-NPs for three (**c**) or seven (**d**) days. * $P < 0.05$.

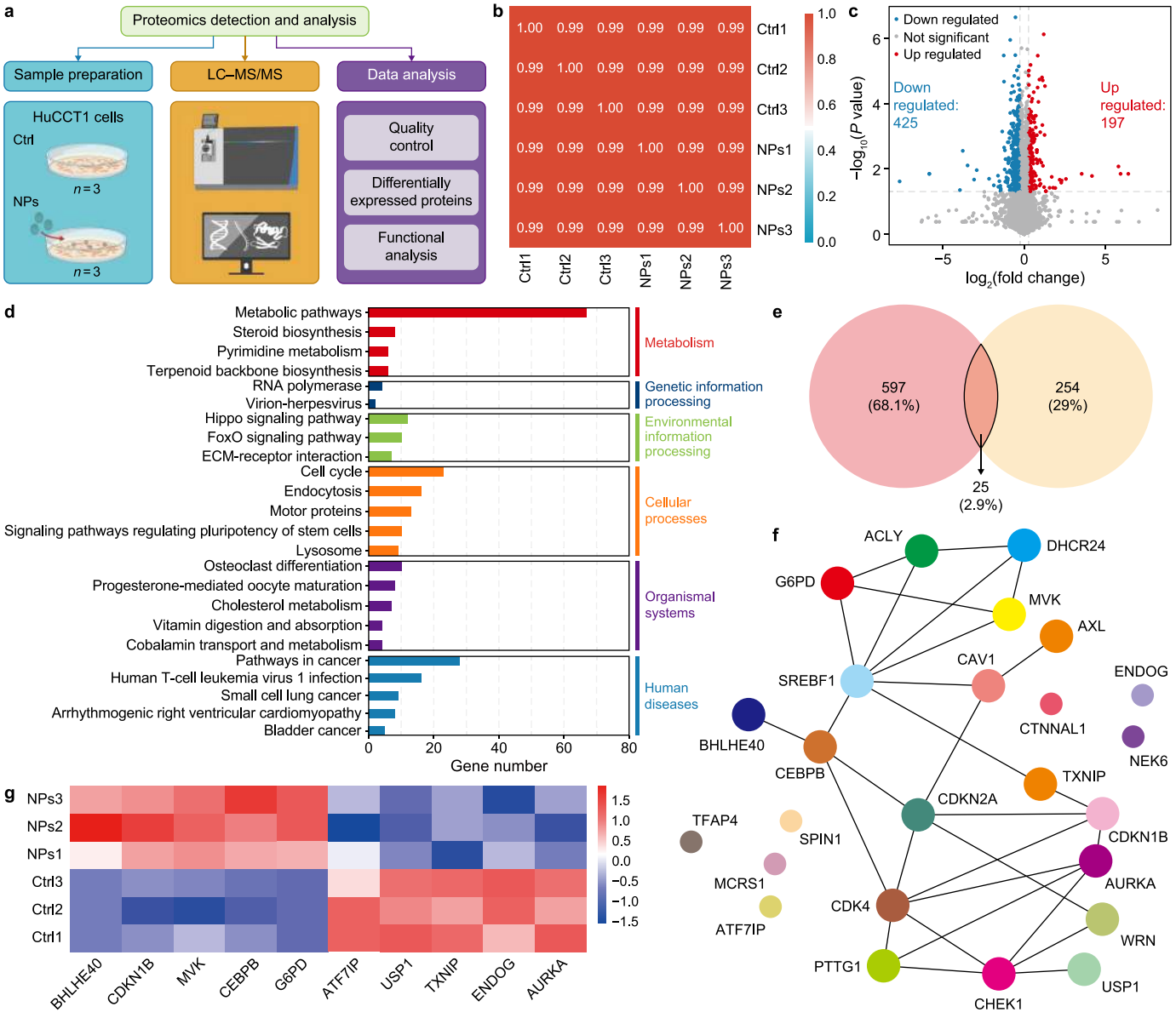

Fig. 6. Proteomic analysis of chronic low-dose polystyrene nanoplastic (PS-NP) exposure-induced cellular sene**scence. a,** Schematic diagram of analyzing the protein expression from the control (Ctrl) and PS-NPs-treated HuCCT1 cells by data-independent acquisition proteomic analysis. **b,** Correlation analysis between Ctrl and PS-NPs-treated HuCCT1 cell samples. **c,** Volcano plot showing the down-regulated proteins (green) and up-regulated proteins (red) in PS-NPs-treated HuCCT1 cells. **d,** Kyoto encyclopedia of genes and genomes (KEGG) pathway enrichment analysis showing the altered pathways. **e,** Venn analysis of PS-NPs-induced differentially expressed proteins with the CellAge database. **f,** Protein–protein interaction network analysis of PS-NPs-regulated proteins was involved in lipid metabolism, transcriptional regulation, and cell cycle processes. **g,** Heatmap analysis of PS-NPs-induced differential expression protein in HuCCT1 cells.

PVC, PET, etc.; 4–30 μm) than healthy individuals, although the role of these MPs in disease progression remains unclear [56]. MPs may disrupt the gut–liver axis by impairing intestinal barrier function and altering microbiome composition, potentially contributing to liver injury [57,58]. These findings highlight widespread human exposure to MP and its potential multiorgan health effects, underscoring the need for further investigation into long-term consequences. The gallbladder bile and the enterohepatic circulation are interdependent. The gallbladder serves as a temporary storage site for bile, while the enterohepatic circulation facilitates the effective utilization of bile salts and the continuous renewal of bile components, thereby promoting the proper functioning of the digestive system. Although bile does not directly interface with the external environment, our findings demonstrate the consistent presence of MPs in all human bile samples, indicating that ingested MPs may enter the enterohepatic circulation and subsequently accumulate in bile. Bile serves not only as a lipid-rich fluid but also as a critical excretory route within the enterohepatic circulation [27]. Dysregulation of key biliary components, such as cholesterol, can lead to precipitation and crystallization in the gallbladder, ultimately promoting gallstone formation [28,29]. Despite this, the role of MPs in gallbladder bile within gut–liver interactions remains poorly understood, and their contribution to gallbladder injury has not yet been fully elucidated.

Notably, this study is the first to identify MPs in human bile samples obtained from 14 donors. Six polymer types were detected: PS (0.87%), PE (27.11%), PP (1.44%), PVC (1.17%), PET (68.05%), and PA66 (1.35%). The concentration of MPs in the bile of gallstone

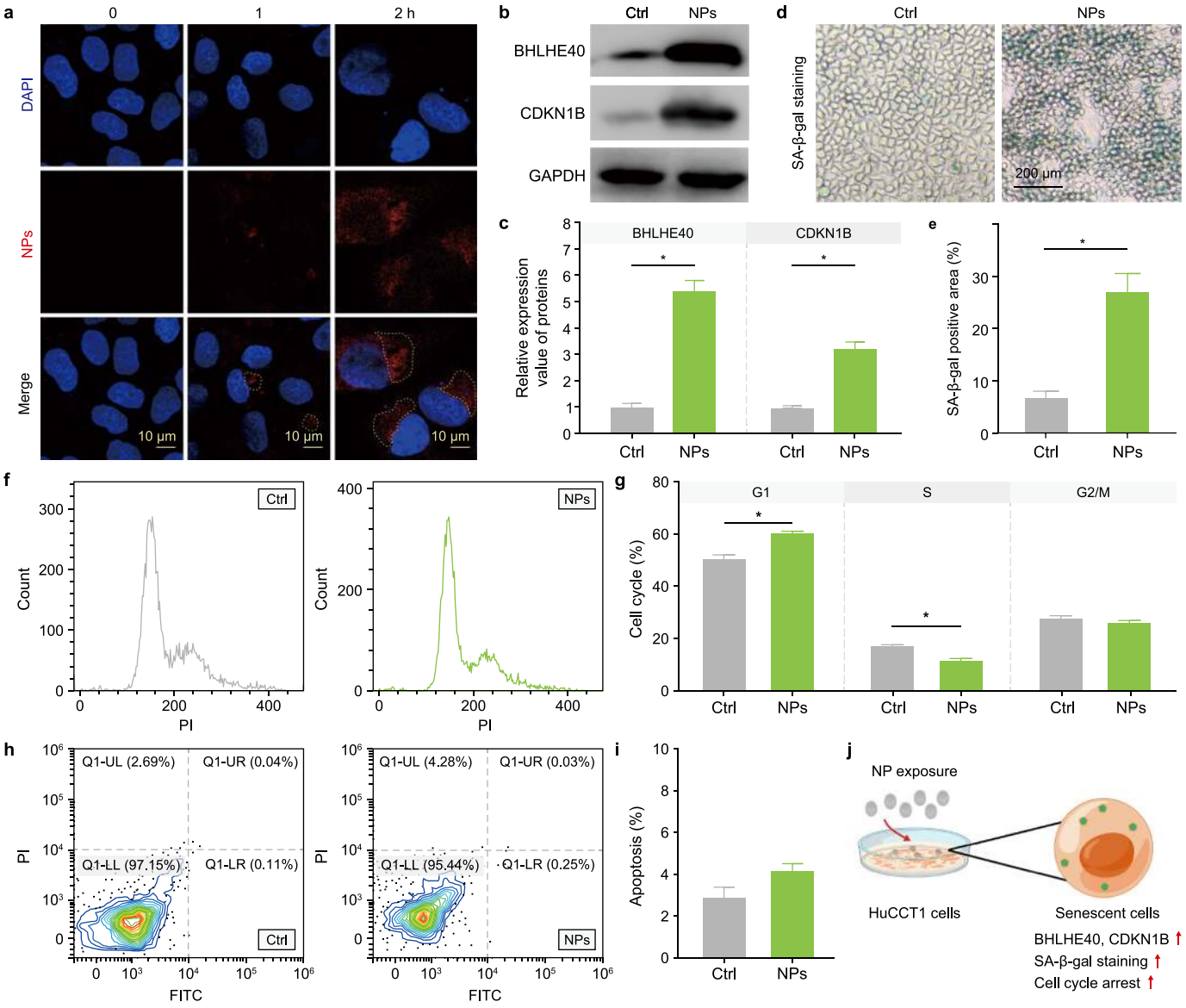

Fig. 7. Chronic low-dose polystyrene nanoplastic (PS-NP) exposure-induced cellular s**enescence. a,** Representative fluorescence images of HuCCT1 cells treated with PS-NPs (red) at 0.04 mg mL^{-1} for 0, 1 and 2 h. Nuclei were stained with DAPI (blue). The area outlined by the dashed box represents a representative region of red fluorescence in the cytoplasm, highlighting the intracellular distribution of PS-NPs. **b–j,** HuCCT1 cells were treated with 0.04 mg mL^{-1} of PS-NPs for seven days. **b,** Protein levels of basic helix-loop-helix family member e40 (BHLHE40) and cyclin dependent kinase inhibitor 1B (CDKN1B) detected by Western blot. Glyceraldehyde-3-phosphate dehydrogenase (GAPDH) served as the internal control. **c,** Relative quantification of BHLHE40 and CDKN1B. **d,** Senescence-associated beta-galactosidase (SA-β-gal) staining of HuCCT1 cells treated with PS-NPs. **e,** Relative quantification of SA-β-gal staining. **f,** Cell cycle distribution was analyzed by flow cytometry. **g,** Quantification of cell cycle distribution. **h,** Cell apoptosis analyzed by flow cytometry. **i,** Quantification of cell apoptosis. **j,** Flow diagram of PS-NPs exposure-induced cellular senescence. Data are expressed as mean ± standard deviation. * $P < 0.05$ compared with the control (Ctrl) group.

patients (25.89 [24.26–29.30] μg g^{-1}) was significantly elevated compared to that in controls (6.98 ± 4.56 μg g^{-1}), suggesting that MPs may alter bile flow dynamics and facilitate the aggregation of cholesterol and MPs, thereby contributing to calculi formation [36]. MPs were predominantly detected as irregular and heterogeneous particles within the 20–50 μm size range. These morphological characteristics may enhance their bioavailability and tissue penetration capacity, facilitating intestinal absorption and subsequent entry into the enterohepatic circulation [59]. Hepatic uptake of MPs can induce inflammatory injury and metabolic dysregulation, leading to their active secretion into bile [23,60]. Moreover, the high concentrations of bile salts and lipids in bile likely promote the micellization and retention of hydrophobic MPs via solubilization and embedding mechanisms, thereby facilitating their accumulation within the biliary tract. This may explain the high detection rates of hydrophobic polymers such as PE and PP in bile. Collectively, these findings suggest that variations in MP composition and abundance across tissues and organs may reflect differences in exposure routes and local physiological environments, highlighting the importance of refining human exposure and risk assessment strategies [61].

Although toxicological studies have demonstrated that MPs can trigger toxic effects such as oxidative stress and immune dysfunction, the direct extrapolation of these findings to human health risk remains challenging due to the significant disparities in dose, polymer composition, and exposure duration compared with real-

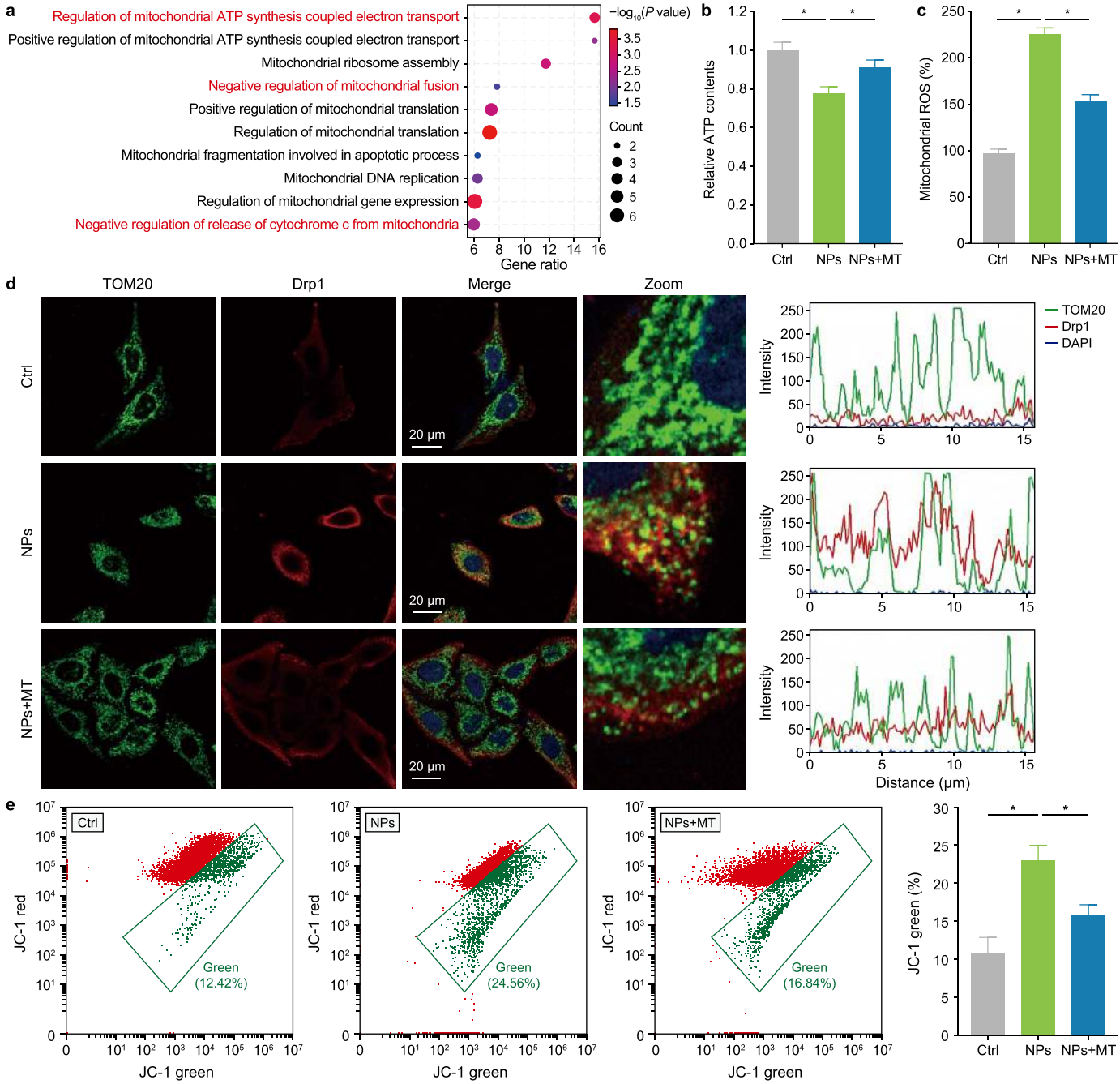

Fig. 8. Melatonin reverses chronic low-dose polystyrene nanoplastic (PS-NP) exposure-induced mitochondrial damage in HuCCT1 **cells. a,** Gene Ontology enrichment analysis was performed for the biological processes of differentially expressed proteins. The red text highlights the mitochondrial-related functions investigated in this study. **b–e,** HuCCT1 cells were treated with 0.04 mg mL^{-1} of PS-NPs individually or combined with melatonin (20 μM) for 7 days. **b**, Detection of adenosine triphosphate (ATP) content in HuCCT1 cells. **c**, Flow cytometric detection of mitochondrial reactive oxygen species (ROS) levels in HuCCT1 cells. **d**, Representative images showing the Drp1 (red) distribution in mitochondria (TOM20, green) of HuCCT1 cells were captured by confocal microscopy (left). Fluorescence curves were generated by Zen 2010 software (right). **e**, Flow cytometric detection of mitochondrial membrane potential in HuCCT1 cells. Cells were treated with Ctrl, NPs, or NPs + MT. JC-1 green fluorescence (depolarized mitochondria) was quantified. Data are expressed as mean ± standard deviation. * $P < 0.05$.

world scenarios of chronic, low-dose exposure to heterogeneous environmental MPs [62,63]. The accumulation of MPs in the biliary system may collectively contribute to pathological changes in the enterohepatic circulation axis through various mechanisms, including physical obstruction, induction of local immune-inflammatory responses, and their role as carriers of toxic chemicals [57,64].

In our study, we simulated real human exposure scenarios using a low-dose, chronic exposure model and screened MPs at different doses and types. The results demonstrated that chronic low-dose MP exposure induces MiDAS. Importantly, we found that melatonin effectively mitigates this toxic effect, suggesting a novel intervention strategy against MP-induced health hazards and providing new insights into human health risk assessment. These results are consistent with previous findings that mitochondrial dysfunction is a major contributor to cellular senescence

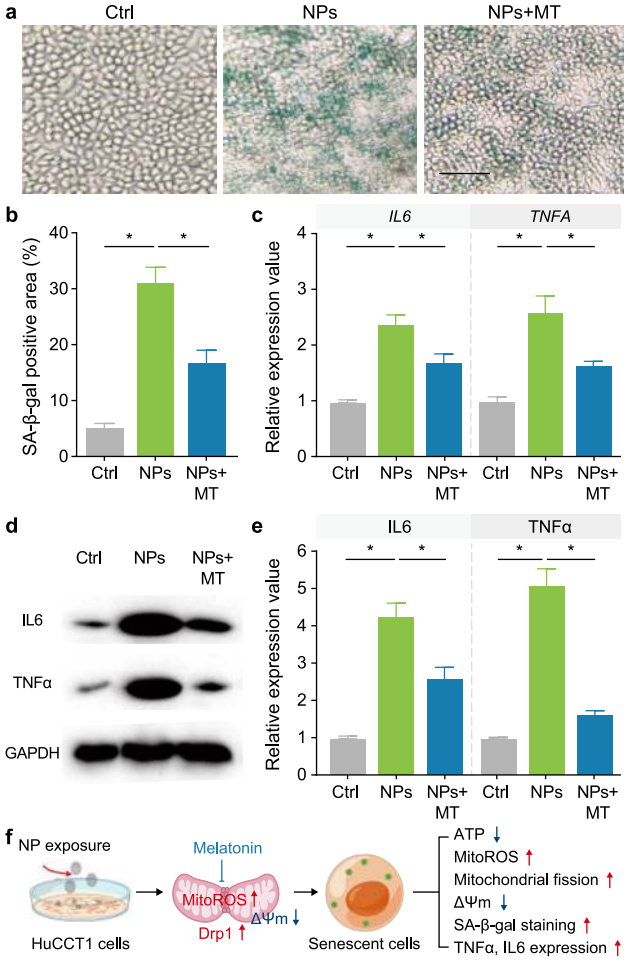

Fig. 9. Melatonin reverses chronic low-dose polystyrene nanoplastic (PS-NP) exposure-induced cellular senescence by inhibiting mitochondrial **damage. a–e,** HuCCT1 cells were treated with 0.04 mg mL^{-1} of PS-NPs individually or combined with melatonin (20 μM) for seven days. **a**, SA-β-gal staining of HuCCT1 cells. **b**, Relative quantification of SA-β-gal staining. **c**, The mRNA levels of *IL6* and *TNFA* detected by qRT-PCR. **d**, The protein levels of IL6 and TNFα detected by Western blot. **e**, Relative quantification of IL6 and TNFα. **f**, Model diagram of melatonin reverses chronic low-dose PS-NPs exposure-induced cellular senescence by inhibiting mitochondrial damage. Data are expressed as mean ± standard deviation. * $P < 0.05$.

[49,65,66]. Of particular importance, our study showed that melatonin antioxidant intervention to reduce intracellular ROS levels and maintain normal mitochondrial function could partially attenuate cellular senescence. Corroborating this finding, research indicates that melatonin can effectively counteract cardiovascular and placental damage induced by $PM_{2.5}$ and environmental stressors by regulating mitochondrial redox homeostasis and suppressing ROS-mediated aberrant autophagy, suggesting melatonin's substantial potential in environmental toxin protection [67,68]. Furthermore, melatonin can upregulate endogenous antioxidant enzyme activities and protect the integrity of barrier organs, such as the gut and liver, by modulating relevant signaling pathways, including Sirt1, thereby providing an innovative scientific hypothesis for its potential to mitigate MP toxicity following oral ingestion [69]. Future studies are urgently needed to elucidate the precise mechanisms by which MPs are transported to and retained within the biliary tract via the enterohepatic circulation.

In conclusion, this study provides evidence of MP accumulation in human bile, revealing significantly higher levels in patients with gallstones. We demonstrate that chronic MP exposure induces MiDAS in cholangiocytes, thereby establishing a novel link between environmental MP pollution and biliary disease. Importantly, our pharmacological findings highlight melatonin's potential to mitigate MP-induced cytotoxicity. Collectively, these results identify the biliary system as a previously unrecognized target of MP exposure and provide a scientific basis for developing environmental policies and clinical intervention strategies to reduce MP-related health risks.

5. Limitations and future perspectives

This study provides evidence of MPs in human bile and explores their potential association with gallstones and underlying mechanisms of toxicity; however, several limitations should be acknowledged. First, the relatively small sample size from a single medical center may limit the generalizability of the findings. Second, assessment of MP exposure routes was incomplete due to the absence of detailed dietary questionnaires, occupational exposure histories, and environmental monitoring data, making it difficult to accurately quantify individual exposure levels. Third, a more comprehensive understanding of MP pollution requires a holistic "microplastome" perspective to systematically characterize its composition and health effects [70]. Additionally, although in vitro experiments confirmed that low-dose MPs induce cholangiocyte senescence via mitochondrial dysfunction, further validation using long-term animal exposure models and human exposure level studies is still needed.

Future research should expand the sample size and incorporate multicenter collaborations to enhance the robustness and reliability of the data. Standardized exposure assessment tools (e.g., detailed dietary surveys, environmental MP monitoring, and occupational history analyses) should be employed to better evaluate the association between MP exposure and biliary diseases. Furthermore, we plan to establish chronic animal exposure models that simulate real-world environmental doses to validate cumulative effects and clarify molecular mechanisms (e.g., mitochondrial damage and cellular senescence). Exploring potential intervention strategies (e.g., mitochondria-targeted therapy) should also be prioritized to provide more comprehensive scientific evidence for clinical and environmental policy-making.

Furthermore, to address practical public health and regulatory needs, a systematic and tiered set of actionable measures should be considered. These include the following:

- Source control: Prohibiting plastic microbeads in cosmetics and personal care products while encouraging the development of biodegradable alternatives and the adoption of cleaner production processes
- Process monitoring: Incorporating MPs as a mandatory parameter in drinking water quality surveillance and promoting advanced treatment technologies such as nanofiltration to improve removal efficiency
- Health protection: Establishing standardized MP risk assessment frameworks and developing exposure guidelines for high-risk populations with biliary tract diseases
- Public engagement: Enhancing environmental awareness via media and educational campaigns to advocate green and low-carbon lifestyles

In addition, we emphasize the importance of advancing the standardization of MP detection methods—drawing on established frameworks such as EUROqCHARM and ISO standards—and developing a comprehensive database of toxic plastic oligomers, thereby providing a solid scientific foundation for evidence-based policy formulation and effective implementation [17].

CRediT authorship contribution statement

Leilei Zhan: Writing – original draft, Investigation, Data curation. **Li Fu:** Data curation, Formal analysis, Investigation, Methodology. **Qingli Zeng:** Formal analysis, Data curation, Investigation. **Ruiyin Liang:** Data curation. **Jinhui Tang:** Data curation. **Juan Liu:** Formal analysis. **Bo Qian:** Writing – review & editing, Conceptualization, Supervision, Validation, Funding acquisition. **Zhe Xu:** Writing – review & editing, Project administration, Funding acquisition, Conceptualization, Supervision. **Lin Che:** Writing – review & editing, Writing – original draft, Visualization, Methodology, Funding acquisition, Conceptualization, Data curation.

Declaration of competing interest

The authors declare that they have no known competing financial interests or personal relationships that could have appeared to influence the work reported in this paper.

Acknowledgements

This work was supported by the National Natural Science Foundation of China (Grant number 82304180, 82460652), Natural Science Foundation of Guangdong Provincial (Grant number 2024A1515010893), Project funded by China Postdoctoral Science Foundation (Grant number 2024T171083, 2024MD763959), Postdoctoral Fellowship Program of CPSF (Grant number GZB20250189), and the Social Science and Technology Development Key Project of Dongguan (Grant number 20211800905292).

Appendix A. Supplementary data

Supplementary data to this article can be found online at https://doi.org/10.1016/j.ese.2026.100686.

References

[1] R. Geyer, J.R. Jambeck, K.L. Law, Production, use, and fate of all plastics ever made, Sci. Adv. 3 (2017) e1700782.
[2] D. Kwon, Three ways to solve the plastics pollution crisis, Nature 616 (2023) 234–237.
[3] J.R. Jambeck, R. Geyer, C. Wilcox, T.R. Siegler, M. Perryman, A. Andrady, R. Narayan, K.L. Law, Marine pollution. Plastic waste inputs from land into the ocean, Science 347 (2015) 768–771.
[4] D.M. Mitrano, P. Wick, B. Nowack, Placing nanoplastics in the context of global plastic pollution, Nat. Nanotechnol. 16 (2021) 491–500.
[5] D. Mohrig, Deep-ocean seafloor islands of plastics, Science 368 (2020) 1055.
[6] A. Zeb, W. Liu, N. Ali, R. Shi, Q. Wang, J. Wang, J. Li, C. Yin, J. Liu, M. Yu, J. Liu, Microplastic pollution in terrestrial ecosystems: global implications and sustainable solutions, J. Hazard. Mater. 461 (2024) 132636.
[7] L.J.W. van der Laan, T. Bosker, W. Peijnenburg, Deciphering potential implications of dietary microplastics for human health, Nat. Rev. Gastroenterol. Hepatol. 20 (2023) 340–341.
[8] M. Suran, Microplastics are found outside in nature and inside the body-but evidence of health risks is inconclusive, JAMA 328 (2022) 911–913.
[9] M. Kozlov, Landmark study links microplastics to serious health problems, Nature (2024).
[10] C.M.C. Richard, E. Dejoie, C. Wiegand, G. Gouesbet, H. Colinet, P. Balzani, D. Siaussat, D. Renault, Plastic pollution in terrestrial ecosystems: current knowledge on impacts of micro and nano fragments on invertebrates, J. Hazard. Mater. 477 (2024) 135299.
[11] B. Zhao, R.E. Richardson, F. You, Microplastics monitoring in freshwater systems: a review of global efforts, knowledge gaps, and research priorities, J. Hazard. Mater. 477 (2024) 135329.
[12] K.D. Cox, G.A. Covernton, H.L. Davies, J.F. Dower, F. Juanes, S.E. Dudas, Human consumption of microplastics, Environ. Sci. Technol. 53 (2019) 7068–7074.
[13] L. Van Cauwenberghe, C.R. Janssen, Microplastics in bivalves cultured for human consumption, Environ. Pollut. 193 (2014) 65–70.
[14] P.S. Bhavsar, M.B. Solanki, Y. Shimada, S.B. Kamble, S.P. Patole, G.B. Kolekar, A.H. Gore, Microplastic contamination in Indian rice: a comprehensive characterization and health risk assessment, J. Hazard. Mater. 480 (2024) 136208.
[15] T.W.L. Lam, A.S.Y. Chow, L. Fok, Human exposure to microplastics via the consumption of nonalcoholic beverages in various packaging materials: the case of Hong Kong, J. Hazard. Mater. 472 (2024) 134575.
[16] X. Guo, L. Wang, X. Wang, D. Li, H. Wang, H. Xu, Y. Liu, R. Kang, Q. Chen, L. Zheng, et al., Discovery and analysis of microplastics in human bone marrow, J. Hazard. Mater. 477 (2024) 135266.
[17] R. Marfella, F. Prattichizzo, C. Sardu, G. Fulgenzi, L. Graciotti, T. Spadoni, N. D'Onofrio, L. Scisciola, R. La Grotta, C. Frige, et al., Microplastics and nanoplastics in atheromas and cardiovascular events, N. Engl. J. Med. 390 (2024) 900–910.
[18] Y. Li, L. Chen, N. Zhou, Y. Chen, Z. Ling, P. Xiang, Microplastics in the human body: a comprehensive review of exposure, distribution, migration mechanisms, and toxicity, Sci. Total Environ. 946 (2024) 174215.
[19] A.J. Nihart, M.A. Garcia, E. El Hayek, R. Liu, M. Olewine, J.D. Kingston, E.F. Castillo, R.R. Gullapalli, T. Howard, B. Bleske, et al., Bioaccumulation of microplastics in decedent human brains, Nat. Med. 31 (2025) 1114–1119.
[20] V.C. Shruti, G. Kutralam-Muniasamy, The human plastiphere: a bioparticulate system challenging microplastic risk assessment and governance, Environ. Sci. Technol. 59 (2025) 24131–24150.
[21] Y.L. Wang, Y.H. Lee, Y.H. Hsu, I.J. Chiu, C.C. Huang, C.C. Huang, Z.C. Chia, C.P. Lee, Y.F. Lin, H.W. Chiu, The kidney-related effects of polystyrene microplastics on human kidney proximal tubular epithelial cells HK-2 and male C57BL/6 mice, Environ. Health Perspect. 129 (2021) 57003.
[22] Y. Deng, H. Chen, Y. Huang, Y. Zhang, H. Ren, M. Fang, Q. Wang, W. Chen, R.C. Hale, T.S. Galloway, D. Chen, Long-term exposure to environmentally relevant doses of large polystyrene microplastics disturbs lipid homeostasis via bowel function interference, Environ. Sci. Technol. 56 (2022) 15805–15817.
[23] K. Zhang, J. Yang, L. Chen, J. He, D. Qu, Z. Zhang, Y. Liu, X. Li, J. Liu, J. Li, X. Xie, Q. Wang, Gut microbiota participates in polystyrene microplastics-induced hepatic injuries by modulating the gut-liver axis, ACS Nano 17 (2023) 15125–15145.
[24] H. Zha, S. Han, R. Tang, D. Cao, K. Chang, L. Li, Polylactic acid micro/nanoplastic-induced hepatotoxicity: investigating food and air sources via multi-omics, Environ. Sci. Ecotechnol. 21 (2024) 100428.
[25] R. Lenz, K. Enders, T.G. Nielsen, Microplastic exposure studies should be environmentally realistic, Proc. Natl. Acad. Sci. USA 113 (2016) E4121–E4122.
[26] F. Lammert, K. Gurusamy, C.W. Ko, J.F. Miquel, N. Mendez-Sanchez, P. Portincasa, K.J. van Erpecum, C.J. van Laarhoven, D.Q. Wang, Gallstones, Nat. Rev. Dis. Primers 2 (2016) 16024.
[27] L. Yu, Y. Liu, S. Wang, Q. Zhang, J. Zhao, H. Zhang, A. Narbad, F. Tian, Q. Zhai, W. Chen, Gut microbiota-bile acid-cholestasis interactions: from mechanisms to probiotic therapeutic strategies, Gut Microbes 15 (2023) 2181930.
[28] Y. Asai, T. Yamada, S. Tsukita, K. Takahashi, M. Maekawa, M. Honma, M. Ikeda, K. Murakami, Y. Munakata, Y. Shirai, et al., Hypoxia-inducible factor 1α activation in steatotic liver promotes cholesterol gallstone formation, Gastroenterology 152 (2017) 1521–1535.e8.
[29] X. Huo, Z. Yu, F. Zhao, Y. Chen, P. Chen, L. Xing, Y. Qiao, Y. Peng, M. Tian, M. Zhou, et al., Aquaporin 8-mediated hepatocyte water transport regulates bile dilution and prevents gallstone formation in mice, J. Hepatol. 82 (2025) 464–479.
[30] C. Nie, Z. Li, T. Yang, J. Zhong, Q. Liu, F. Mi, J. Yu, Y. Pan, H. Kan, F. Hong, Associations of long-term exposure to particulate matter with gallstone risks in Chinese adults: a large cross-sectional study, Ecotoxicol. Environ. Saf. 252 (2023) 114644.
[31] A. Parviainen, C. Marchesi, J.M. Suarez-Grau, C.J. Garrido, R. Perez-Lopez, J.M. Nieto, G. Cobo-Cardenas, Unraveling the impact of chronic exposure to metal pollution through human gallstones, Sci. Total Environ. 624 (2018) 1031–1040.
[32] D. Piovani, G.K. Nikolopoulos, A. Aghemo, A. Lleo, S.A. Alqahtani, C. Hassan, A. Repici, S. Bonovas, Environmental risk factors for gallbladder cancer: field-wide systematic review and meta-analysis, Clin. Gastroenterol. Hepatol. (2024).
[33] E. Fournier, M. Leveque, P. Ruiz, J. Ratel, C. Durif, S. Chalancon, F. Amiard, M. Edely, V. Bezirard, E. Gaultier, et al., Microplastics: what happens in the human digestive tract? First evidences in adults using in vitro gut models, J. Hazard. Mater. 442 (2023) 130010.
[34] B. Liang, Y. Deng, Y. Zhong, X. Chen, Y. Huang, Z. Li, X. Huang, X. Yang, J. Du, R. Ye, et al., Gastrointestinal incomplete degradation exacerbates neurotoxic effects of PLA microplastics via oligomer nanoplastics formation, Adv. Sci. (Weinh.) 11 (2024) e2401009.
[35] H. Sun, X. Su, J. Mao, Y. Liu, G. Li, Q. Du, Microplastic detection in maternal blood, fetal appendages, and umbilical vein blood, Ecotoxicol. Environ. Saf. 287 (2024) 117300.
[36] D. Zhang, C. Wu, Y. Liu, W. Li, S. Li, L. Peng, L. Kang, S. Ullah, Z. Gong, Z. Li, et al., Microplastics in human gallstones: detection and formation of cholesterol-microplastic heteroaggregates, J. Hazard. Mater. 467 (2024) 133631.
[37] Z. Huang, B. Hu, H. Wang, Analytical methods for microplastics in the environment: a review, Environ. Chem. Lett. 21 (2023) 383–401.
[38] S. Liu, C. Wang, Y. Yang, Z. Du, L. Li, M. Zhang, S. Ni, Z. Yue, K. Yang, Y. Wang, et al., Microplastics in three types of human arteries detected by pyrolysis-gas chromatography/mass spectrometry (Py-GC/MS), J. Hazard. Mater. 469 (2024) 133855.
[39] L. Zhu, Z. Wu, J. Dong, S. Zhao, J. Zhu, W. Wang, F. Ma, L. An, Unveiling small-

sized plastic particles hidden behind large-sized ones in human excretion and their potential sources, Environ. Sci. Technol. 58 (2024) 11901–11911.
[40] C. Fang, L. Zhao, R. Pu, Y. Lei, W. Zhou, J. Hu, X. Zhang, R. Naidu, Microplastics and nanoplastics released from injection syringe, solid and liquid dimethylpolysiloxane (PDMS), J. Hazard. Mater. 474 (2024) 134782.
[41] N.P. Ivleva, Chemical analysis of microplastics and nanoplastics: challenges, advanced methods, and perspectives, Chem. Rev. 121 (2021) 11886–11936.
[42] T. Wang, Z. Yi, X. Liu, Y. Cai, X. Huang, J. Fang, R. Shen, W. Lu, Y. Xiao, W. Zhuang, S. Guo, Multimodal detection and analysis of microplastics in human thrombi from multiple anatomically distinct sites, EBioMedicine 103 (2024) 105118.
[43] S. Liu, X. Liu, J. Guo, R. Yang, H. Wang, Y. Sun, B. Chen, R. Dong, The association between microplastics and microbiota in placentas and meconium: the first evidence in humans, Environ. Sci. Technol. 57 (2023) 17774–17785.
[44] H. Yu, H. Li, C. Cui, Y. Han, Y. Xiao, B. Zhang, G. Li, Association between blood microplastic levels and severity of extracranial artery stenosis, J. Hazard. Mater. 480 (2024) 136211.
[45] D. Ke, J. Zheng, X. Liu, X. Xu, L. Zhao, Y. Gu, R. Yang, S. Liu, S. Yang, J. Du, B. Chen, G. He, R. Dong, Occurrence of microplastics and disturbance of gut microbiota: a pilot study of preschool children in Xiamen, China, EBioMedicine 97 (2023) 104828.
[46] L. Lv, L. He, S. Jiang, J. Chen, C. Zhou, J. Qu, Y. Lu, P. Hong, S. Sun, C. Li, In situ surface-enhanced Raman spectroscopy for detecting microplastics and nanoplastics in aquatic environments, Sci. Total Environ. 728 (2020) 138449.
[47] D.M. Chitimus, M.R. Popescu, S.E. Voiculescu, A.M. Panaitescu, B. Pavel, L. Zagrean, A.M. Zagrean, MT 'S impact on antioxidative and anti-inflammatory reprogramming in homeostasis and disease, Biomolecules 10 (2020).
[48] H. Pi, S. Xu, R.J. Reiter, P. Guo, L. Zhang, Y. Li, M. Li, Z. Cao, L. Tian, J. Xie, et al., SIRT3-SOD2-mROS-dependent autophagy in cadmium-induced hepatotoxicity and salvage by melatonin, Autophagy 11 (2015) 1037–1051.
[49] Y. Huang, B. Liang, Z. Li, Y. Zhong, B. Wang, B. Zhang, J. Du, R. Ye, H. Xian, W. Min, et al., Polystyrene nanoplastic exposure induces excessive mitophagy by activating AMPK/ULK1 pathway in differentiated SH-SY5Y cells and dopaminergic neurons in vivo, Part. Fibre Toxicol. 20 (2023) 44.
[50] Castroviejo D. Acuna, L.C. Lopez, G. Escames, A. Lopez, J.A. Garcia, R.J. Reiter, Melatonin-mitochondria interplay in health and disease, Curr. Top. Med. Chem. 11 (2011) 221–240.
[51] N. Ali, J. Katsouli, E.L. Marczylo, T.W. Gant, S. Wright, J. Bernardino de la Serna, The potential impacts of micro-and-nano plastics on various organ systems in humans, EBioMedicine 99 (2024) 104901.
[52] G.F. Vasse, B.N. Melgert, Microplastic and plastic pollution: impact on respiratory disease and health, Eur. Respir. Rev. 33 (2024).
[53] M. Liu, J. Mu, M. Wang, C. Hu, J. Ji, C. Wen, D. Zhang, Impacts of polypropylene microplastics on lipid profiles of mouse liver uncovered by lipidomics analysis and Raman spectroscopy, J. Hazard. Mater. 458 (2023) 131918.
[54] V.L.L. S, C.R. Liddle, C.A. Atherall, E. Chapman, M. Watkins, D.J.C. S, J.M. Rotchell, Microplastics in human blood: polymer types, concentrations and characterisation using muFTIR, Environ. Int. 188 (2024) 108751.
[55] L.F. Amato-Lourenco, R. Carvalho-Oliveira, G.R. Junior, Galvao L. Dos Santos, R.A. Ando, T. Mauad, Presence of airborne microplastics in human lung tissue, J. Hazard. Mater. 416 (2021) 126124.
[56] T. Horvatits, M. Tamminga, B. Liu, M. Sebode, A. Carambia, L. Fischer, K. Puschel, S. Huber, E.K. Fischer, Microplastics detected in cirrhotic liver tissue, EBioMedicine 82 (2022) 104147.
[57] X. Wang, K. Deng, P. Zhang, Q. Chen, J.T. Magnuson, W. Qiu, Y. Zhou, Microplastic-mediated new mechanism of liver damage: from the perspective of the gut-liver axis, Sci. Total Environ. 919 (2024) 170962.
[58] J. Wen, H. Sun, B. Yang, E. Song, Y. Song, G. Jiang, Environmentally relevant concentrations of microplastic exposure cause cholestasis and bile acid metabolism dysregulation through a gut-liver loop in mice, Environ. Sci. Technol. 58 (2024) 1832–1841.
[59] R. Xu, J.W. Cao, H.L. Lv, Y. Geng, M.Y. Guo, Polyethylene microplastics induce gut microbiota dysbiosis leading to liver injury via the TLR2/NF-κB/NLRP3 pathway in mice, Sci. Total Environ. 917 (2024) 170518.
[60] W. Zhou, W. Shi, X. Du, Y. Han, Y. Tang, S. Ri, K. Ju, T. Kim, L. Huang, W. Zhang, Y. Yu, D. Tian, Y. Yu, L. Chen, Z. Wu, G. Liu, Assessment of nonalcoholic fatty liver disease symptoms and gut-liver axis status in zebrafish after exposure to polystyrene microplastics and oxytetracycline, alone and in combination, Environ. Health Perspect. 131 (2023) 47006.
[61] M.H. Lamoree, J. van Boxel, F. Nardella, K.J. Houthuijs, S.H. Brandsma, F. Béen, M.B.M. van Duursen, Health impacts of microplastic and nanoplastic exposure, Nat. Med. 31 (2025) 2873–2887.
[62] Z. Yang, G.M. DeLoid, H. Zarbl, J. Baw, P. Demokritou, Micro- and nanoplastics (MNPs) and their potential toxicological outcomes: state of science, knowledge gaps and research needs, NanoImpact 32 (2023) 100481.
[63] S. Wan, X. Wang, W. Chen, M. Wang, J. Zhao, Z. Xu, R. Wang, C. Mi, Z. Zheng, H. Zhang, Exposure to high dose of polystyrene nanoplastics causes trophoblast cell apoptosis and induces miscarriage, Part. Fibre Toxicol. 21 (2024) 13.
[64] H. Xu, J. Wang, Q. Wang, W. Tu, Y. Jin, Co-exposure to polystyrene microplastics and cypermethrin enhanced the effects on hepatic phospholipid metabolism and gut microbes in adult zebrafish, J. Hazard. Mater. 465 (2024) 133051.
[65] S. Lin, H. Zhang, C. Wang, X.L. Su, Y. Song, P. Wu, Z. Yang, M.H. Wong, Z. Cai, C. Zheng, Metabolomics reveal nanoplastic-induced mitochondrial damage in human liver and lung cells, Environ. Sci. Technol. 56 (2022) 12483–12493.
[66] W. Jin, W. Zhang, H. Tang, P. Wang, Y. Zhang, S. Liu, J. Qiu, H. Chen, L. Wang, R. Wang, et al., Microplastics exposure causes the senescence of human lung epithelial cells and mouse lungs by inducing ROS signaling, Environ. Int. 185 (2024) 108489.
[67] J. Jiang, S. Liang, J. Zhang, Z. Du, Q. Xu, J. Duan, Z. Sun, Melatonin ameliorates PM2.5-induced cardiac perivascular fibrosis through regulating mitochondrial redox homeostasis, J. Pineal Res. 70 (2021) e12686.
[68] H.L. Zhu, X.T. Shi, X.F. Xu, G.X. Zhou, Y.W. Xiong, S.J. Yi, W.B. Liu, L.M. Dai, X.L. Cao, D.X. Xu, H. Wang, Melatonin protects against environmental stress-induced fetal growth restriction via suppressing ROS-mediated GCN2/ATF4/BNIP3-dependent mitophagy in placental trophoblasts, Redox Biol. 40 (2021) 101854.
[69] W. Rungratanawanich, K.R. LeFort, Y.E. Cho, X. Li, B.J. Song, Melatonin prevents thioacetamide-induced gut leakiness and liver fibrosis through the gut-liver axis via modulating Sirt1-related deacetylation of gut junctional complex and hepatic proteins, J. Pineal Res. 76 (2024) e13007.
[70] C. Li, X. Li, M.S. Bank, T. Dong, J.K. Fang, F.D.L. Leusch, M.C. Rillig, J. Wang, L. Wang, Y. Xia, E.G. Xu, Y. Yang, C. Zhang, D. Zhu, J. Liu, L. Jin, The "Microplastome" - a holistic perspective to capture the real-world ecology of microplastics, Environ. Sci. Technol. 58 (2024) 4060–4069.